"Optimizing Energy Efficiency and Performance in High-Performance Computing through Advanced Direct-to-Chip Liquid Cooling and LabVIEW-Based Monitoring and Analysis"

by

Chandraprakash Ashok Hinge

DISSERTATION

Submitted in partial fulfillment of the requirements
for the degree of Doctor of Philosophy at
The University of Texas at Arlington
December 2023

Arlington, Texas

Supervising Committee:

Dereje Agonafer, Supervising Professor
Abdolhossein Haji-Sheikh
Dr. Amaya Miguel A
Dr. Sunand Santhanagopalan
Dr. Pardeep Shahi

Acknowledgments

I am sincerely indebted to my sister **Ashwini Hinge** and my parents **Sunanda Ashok Hinge** for their unwavering and indispensable support throughout my pursuit of higher education in the United States. Their encouragement and belief in my abilities have been the driving force behind my academic journey.

I extend my heartfelt thanks to **Dr. Agonafer,** who generously provided me with the chance to undertake a Ph.D. under his expert guidance. His consistent mentorship has not only shaped my research but has also been a source of inspiration throughout this academic endeavor. Dr. Agonafer's dedication as an exceptional advisor has played a pivotal role in my academic growth.

I express my deep appreciation to the committee members **Dr.Haji-Sheikh, Dr.Amaya, Dr.Sunand, and Dr.Shahi** for their vital role in overseeing and evaluating my dissertation defense. Their insightful feedback and guidance have significantly contributed to the refinement of my research.

A special note of gratitude goes to the NVIDIA team for their sponsorship of this project. Their support has provided me with the resources and opportunities essential for conducting meaningful research. This collaboration has been instrumental in the success of my doctoral journey.

Lastly, I want to express my thanks to my friends whose companionship has made this challenging doctoral journey incredibly enjoyable. Their encouragement, camaraderie, and shared experiences have added a significant dimension of joy to this academic pursuit, and for that, I am truly grateful.

Dedication

I would like to extend my heartfelt dedication to this doctoral thesis to my cherished late grandfather, Haribhau Hinge, and my maternal grandfather, Sitaram Mengade. Since the day I was born, both of you have held a special place in my heart, being constant in my life. This dedication is a tribute to the profound impact you have had on my personal and academic journey.

To my late grandfather, Haribhau Hinge, your wisdom, love, and support have been guiding lights even in your physical absence. Your memory lives on in the lessons you imparted and the values you instilled in me. This thesis serves as a tribute to the enduring influence you have had on my character and aspirations.

To my maternal grandfather, Sitaram Mengade, I am grateful for your continued presence, love, and encouragement. Your unwavering support has been a source of strength throughout my academic pursuit. This dedication is a celebration of the living bond we share and the inspiration I draw from your enduring guidance.

Together, both of you represent the pillars of strength in my life, and I carry your collective influence with deep gratitude. This thesis is not only an academic achievement but also a testament to the profound impact of familial support and love on one's journey of growth and learning.

Abstract

Optimizing Energy Efficiency and Performance in High-Performance Computing through Advanced Direct-to-Chip Liquid Cooling and LabVIEW-Based Monitoring and Analysis

Chandraprakash Ashok Hinge

The University of Texas at Arlington, 2023

Supervising Professor: Dereje Agonafer

This research endeavors to significantly enhance energy efficiency and performance in the realm of high-performance computing (HPC). This goal is pursued through a synergistic approach that leverages advanced direct-to-chip liquid cooling systems and integrates LabVIEW for real-time monitoring and analysis within data centers.

The primary aims of this study are manifold. First, it seeks to evaluate the effectiveness of different single-phase liquid coolants when employed in direct-to-chip cold plate cooling for HPC systems. Additionally, the research focuses on characterizing row manifolds, crucial elements in the design of efficient data centers. The study also endeavors to devise a strategic control mechanism that ensures stability in secondary supply temperature, particularly at very low loads. Further, the development of a LabVIEW-based software solution for efficient data logging and analysis forms an integral part of the study's objectives.

In the current landscape, the surge in demand for high-performance computing, propelled by technologies such as AI, IoT, and machine learning, necessitates advancements in thermal management strategies. The research pays specific attention to the efficacy of direct-to-chip liquid cooling in mitigating challenges associated with thermal design power and form factors within HPC systems. It distinguishes itself by conducting a thorough and comprehensive evaluation of various single-phase liquid coolants, emphasizing their performance and reliability under diverse conditions. Furthermore, the study sets itself apart by delving into the characterization of row manifolds, a critical aspect of optimizing data center design. The integration of LabVIEW for real-time monitoring introduces a unique and valuable dimension to this research.

At its core, this study is driven by the urgent need for efficient cooling solutions to counter the significant thermal power generated by high-end CPUs and GPUs. Direct-to-chip liquid cooling emerges as a viable solution due to its inherent efficiency. The study endeavors to scrutinize a

range of liquid coolants to optimize thermal performance and provide a reliable cooling approach for HPC systems.

Reflecting on the progress made thus far, the preliminary work has been substantial. It encompassed a thorough literature review and the setup of experimental configurations to evaluate coolant performance and characterize row manifolds. Furthermore, a strategic control mechanism was developed to stabilize the secondary supply temperature, even at exceedingly low loads. Additionally, a software solution leveraging LabVIEW was crafted to efficiently log and analyze data, a crucial step toward streamlined data center management.

Looking ahead, the research will delve into a more comprehensive set of experiments to evaluate the reliability and long-term performance of selected single-phase liquid coolants. A specific focus will be placed on examining propylene glycols at concentrations of 25%. This entails an in-depth analysis of the effectiveness of corrosion inhibitors, employing standardized testing apparatus. Additionally, the meticulously gathered experimental data will undergo thorough analysis. This analysis is expected to facilitate the calculation of the Total Cost of Ownership (TCO) associated with each coolant. Insights gleaned from this calculation will shed light on the economic implications of coolant selection at the data center level. Simultaneously, the LabVIEW-based software solution will undergo further validation, fine-tuning, and optimization. This iterative process aims to ensure seamless integration into data center management processes, ultimately bolstering operational efficiency and reliability.

In conclusion, the remaining work holds significant promise, aligned closely with the study's objectives. It promises to offer a comprehensive understanding of coolant reliability, economic considerations in coolant selection, and the augmentation of data center operational efficiency through advanced data logging and analysis.

Abbreviations

HPC	High Performance Computing
AI	Artificial Intelligence
IoT	Internet of Things
DCLC	Direct Chip Liquid Cooling
CPU	Central Processing Unit
GPU	Graphic Processing Unit
TCO	Total Cost of Ownership
PG	Propylene Glycol
EG	Ethylene Glycol
DI	Deionized
TTV	Thermal Test Vehicle
Rth	Thermal Resistance
ΔP	Pressure Drop
LPM	Liters Per Minute
PSI	Pounds per Square Inch
TDP	Thermal Design Power
FNM	Flow Network Modeling
DAQs	Data Acquisition System
GAR	Graphical Analysis of Risks
ASTM	American Society for Testing and Materials
Q	Heat Load

EPDM	Ethylene Propylene Diene Monomer
Cu	Copper
CDU	Coolant Distribution Unit
OCP	Open Compute Project
ASHRAE	American Society of Heating, Refrigeration and Air Conditioning Engineers

List of Illustrations

List of Tables

Table of Contents

Chapter 1

Introduction

Data centers, the cornerstone of modern computing infrastructures, house vast arrays of servers, each laden with electronic components generating substantial heat. The continuous demand for high-performance computing (HPC), propelled by technologies such as artificial intelligence (AI), the Internet of Things (IoT), and machine learning, has led to an unprecedented surge in computational requirements. The consequential increase in transistor density within CPUs and GPUs has given rise to elevated thermal dissipation and heat flux, necessitating effective thermal management strategies. Figure 1.1 shows trends in microprocessors in recent years.
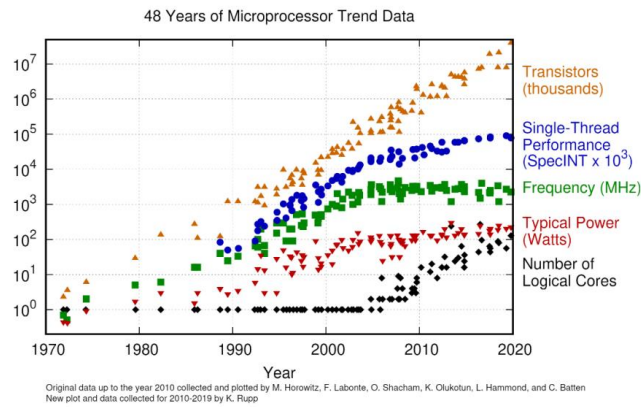
FIGURE 1.1: MICROPROCESSOR TRENDS IN RECENT YEARS [1]

The importance of thermal management in data centers is underscored by the current energy consumption trends. Data centers in the United States currently consume 2% of the total electricity, a figure projected to reach 73 billion kWh in 2020 and a predicted 180 billion kWh by 2050. Air cooling, the conventional approach, is proving less efficient at higher temperatures, prompting a need for advanced cooling technologies to minimize thermal resistance and optimize overall efficiency. Figure 1.2 illustrates data center energy consumption.
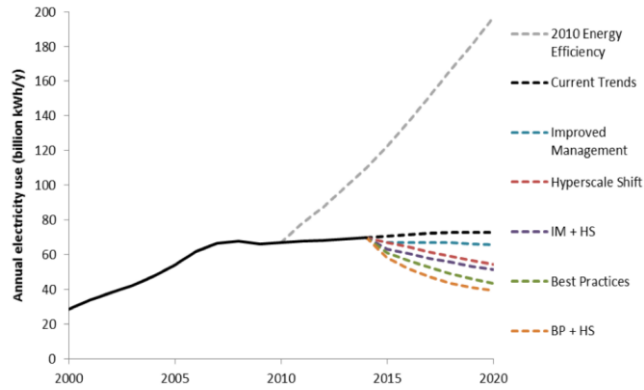
FIGURE 1.2: PRESENTED DATA CENTER ENERGY CONSUMPTION[1]

This research endeavors to address these challenges by significantly enhancing energy efficiency and performance in the realm of HPC. The approach taken is synergistic, leveraging advanced direct-to-chip liquid cooling systems and integrating LabVIEW for real-time monitoring and analysis within data centers.

The primary objectives of this study are multi-faceted. Firstly, it aims to evaluate the effectiveness of different single-phase liquid coolants in direct-to-chip cold plate cooling for HPC systems. Additionally, the research focuses on characterizing row manifolds, crucial elements in the design of efficient data centers. The study also aims to devise a strategic control mechanism ensuring stability in secondary supply temperature, particularly at very low loads. Furthermore, the development of a LabVIEW-based software solution for efficient data logging and analysis forms an integral part of the study's objectives.

The surge in demand for high-performance computing necessitates advancements in thermal management strategies. This research pays specific attention to the efficacy of direct-to-chip liquid cooling in mitigating challenges associated with thermal design power and form factor within HPC systems. It distinguishes itself through a comprehensive evaluation of various single-phase liquid coolants, emphasizing their performance and reliability under diverse conditions. The study sets itself apart by delving into the characterization of row manifolds, a critical aspect for optimizing data center design. The integration of LabVIEW for real-time monitoring introduces a unique and valuable dimension to this research.

At its core, this study responds to the urgent need for efficient cooling solutions to counter the significant thermal power generated by high-end CPUs and GPUs. Direct-to-chip liquid cooling emerges as a viable solution due to its inherent efficiency. The study scrutinizes a range of liquid coolants to optimize thermal performance and provide a reliable cooling approach for HPC systems.

Reflecting on the progress made thus far, the preliminary work encompassed a thorough literature review and the setup of experimental configurations to evaluate coolant performance and characterize row manifolds. Furthermore, a strategic control mechanism was developed to stabilize the secondary supply temperature, even at exceedingly low loads. Additionally, a software solution leveraging LabVIEW was crafted to efficiently log and analyze data, a crucial step toward streamlined data center management.

Looking ahead, the research will delve into a more comprehensive set of experiments to evaluate the reliability and long-term performance of selected single-phase liquid coolants. Specific focus will be placed on examining propylene glycols at concentrations of 25%. This entails an in-depth analysis of the effectiveness of corrosion inhibitors, employing standardized testing apparatus. Additionally, the gathered experimental data will undergo thorough analysis, facilitating the calculation of the Total Cost of Ownership (TCO) associated with each coolant.

In conclusion, the remaining work holds significant promise, aligned closely with the study's objectives. It promises to offer a comprehensive understanding of coolant reliability, economic considerations in coolant selection, and the augmentation of data center operational efficiency through advanced data logging and analysis. This research aims to contribute valuable insights towards the sustainable advancement of high-performance computing in the evolving landscape of data centers.

Chapter 2

Literature Review

The demand for high-performance data centers has surged in the past decade, driven by the increasing computational requirements of modern applications. Cooling high-computing processors has emerged as a significant challenge, prompting a shift from traditional air cooling to more efficient liquid cooling methods. In a groundbreaking study by IBM [9], liquid cooling demonstrated an efficiency boost of almost 3500 times compared to forced air cooling. Liquid cooling, especially microchannel-based approaches, has been recognized for its higher heat transfer removal coefficient, making it a promising solution [2][3][4].

Research efforts have delved into optimizing liquid cooling, particularly with a direct-to-chip approach, ranging from single cold plate performance testing to rack-level examinations [5]. Analytical models, such as the top in/side exit (TISE) or split flow cold plates, have been developed and validated to enhance thermo-hydraulic performance [6]. Computational Fluid Dynamics (CFD) studies have further optimized the shape of split flow cold plates, considering the effects of inlet and outlet manifolds [7-9]. Additionally, numerical modeling has explored warm water-cooled microchannel V-grooved impinged cold plates, offering insights into pressure drop and thermal resistance [10]. Targeted coolant delivery for microchannel heatsinks has also been investigated, proposing designs that reduce thermal resistance significantly [11].

In the realm of indirect liquid cooling, hybrid approaches incorporating both liquid and air cooling have been explored [12]. The feasibility of rear door heat exchangers (RDHx) has been demonstrated, providing guidelines for their implementation based on heat load and server design [13]. Detailed analytical and numerical simulations, including the development of system calculators, have been undertaken to analyze entire liquid-to-liquid cooling systems [14][15]. Another study delved into the corrosion mechanism for copper-based cold plates, considering factors like fluid temperature, type, and galvanic potential [16].

Liquid coolants, integral components of cooling loops, must meet specific criteria for optimal performance. They need to be non-flammable, economical, non-toxic, and compatible with wetted materials such as metals and polymers. Furthermore, coolants must exhibit excellent thermo-physical properties, including low viscosity, high specific heat, and thermal conductivity. Deionized water, with its exceptional thermal conductivity, is a common coolant in the industry. However, its freezing point and expansion upon freezing pose challenges, prompting the addition of glycols to mitigate these issues. Propylene and ethylene glycols are commonly used freeze point depressants, but they can reduce heat transfer efficiency compared to water. Additionally, corrosion inhibitors are crucial to prevent degradation of wetted components and potential system failures due to fluid leakage or channel blockage [17][18][19][20].

Industry recommendations, such as those from ASHRAE and the Open Compute Project (OCP), provide valuable guidance on mitigating corrosion risks. Propylene glycol and ethylene glycol are recommended for their lower corrosivity. OCP specifically recommends propylene glycol-containing fluids for their corrosion inhibition properties, addressing concerns in copper corrosion.

Monitoring pH values and aluminum ion concentrations in coolants is highlighted as a proactive measure against corrosion risks [21][22].

In the context of software solutions for data center management, there is a pressing need to address the challenges associated with cooling technologies. Efficient cooling is essential not only for optimal performance but also for energy efficiency and reliability. Recent research has proposed a LabVIEW-based software solution for automating data logging and analysis in data centers [LabVIEW Research]. This innovative approach aims to enhance operational efficiency and streamline management processes by leveraging LabVIEW's capabilities in system design and automation. The integration of LabVIEW-based solutions with dynamic cooling strategies could potentially offer a comprehensive approach to data center management, combining real-time monitoring, automation, and dynamic adjustments for improved efficiency.

In summary, the convergence of advances in liquid cooling technologies and the development of sophisticated software solutions presents a promising path towards achieving optimal data center performance, energy efficiency, and reliability. The subsequent sections delve into specific areas of research, including the selection and evaluation of liquid coolants and the comparison and evaluation of different types of single-phase liquid coolants in direct-to-chip cold plate-based liquid cooling systems. These insights aim to inform decision-making at the data center level, providing a holistic perspective on cooling efficiency optimization.

Chapter 3

Thermal and Hydraulic testing of single-phase cold plate-based coolants

3.1 Abstract

Due to the increasing computational demand driven by artificial intelligence, machine learning, and the Internet of Things (IoT), there has been an unprecedented growth in transistor density for high-end CPUs and GPUs. This growth has resulted in high thermal dissipation power (TDP) and high heat flux, necessitating the adoption of advanced cooling technologies to minimize thermal resistance and optimize cooling efficiency. Among these technologies, direct-to-chip cold plate-based liquid cooling has emerged as a preferred choice in electronics cooling due to its efficiency and cost- effectiveness. In this context, different types of single-phase liquid coolants, such as propylene glycol (PG), ethylene glycol (EG), DI water, treated water, and nanofluids, have been utilized in the market. These coolants, manufactured by different companies, incorporate various inhibitors and chemicals to enhance long-term performance, prevent bio- growth, and provide corrosion resistance. However, the additives used in these coolants can impact their thermal performance, even when the base coolant is the same. This paper aims to compare these coolant types and evaluate the performance of the same coolant from different vendors. The selection of coolants in this study is based on their performance, compatibility with wetted materials, reliability during extended operation, and environmental impact, following the guidelines set by ASHRAE. To conduct the experiments, a single cold plate-based benchtop setup was constructed, utilizing a thermal test vehicle (TTV), pump, reservoir, flow sensor, pressure sensors, thermocouple, data acquisition units, and heat exchanger.

Each coolant was tested using a dedicated cold plate, and thorough cleaning procedures were carried out before each experiment. The experiments were conducted under consistent boundary conditions, with a TTV power of 1000 watts and varying coolant flow rates (ranging from 0.5 lpm to 2 lpm) and supply coolant temperatures (17°C, 25°C, 35°C, and 45°C), simulating warm water cooling. The thermal resistance (Rth) versus flow rate and pressure drop (ΔP) versus flow rate graphs were obtained for each coolant, and the impact of different supply coolant temperatures on pressure drop was characterized. The data collected from this study will be utilized to calculate the Total Cost of Ownership (TCO) in future research, providing insights into the impact of coolant selection at the data center level. There is limited research available on the reliability used in direct-to-chip liquid cooling, and there is currently no standardized methodology for testing their reliability. This study aims to fill this gap by focusing on the reliability of coolants, specifically propylene glycols at concentrations of 25%. To analyze the effectiveness of corrosion inhibitors in these coolants, ASTM standard D1384 apparatus, typically used for testing engine coolant corrosion inhibitors on metal samples in controlled laboratory settings, was employed. The setup involved immersing samples of wetted materials (copper, solder coated brass, brass, stainless steel, cast iron, and cast aluminum) in separate jars containing inhibited propylene glycol solutions from

different vendors. This test will determine the reliability difference between the same inhibited solutions from different vendors.

Keywords: Data Center, Direct-to-chip liquid cooling, coolants, thermal performance, reliability

3.2 MATERIALS AND METHODS

This chapter is divided into two main categories, first we discuss about the coolant's thermal and hydraulic testing where the thermal test vehicle, experimental setup, different coolants, cleaning procedure and methodology are discussed briefly, and in the second part briefly describes about the coolant's reliability testing using the ASTM test setup recommended in OCP guidelines.

3.2.1. COOLANT THERMAL AND HYDRAULIC TESTING

3.2.1.1. DESCRIPTION OF TTV MODULE

A thermal testing vehicle is a machine that simulates a data center server environment to assess the effectiveness of various cooling technologies. The vehicle is intended to mimic the case temperature and ambient conditions that a data center server would encounter, allowing for reliable testing and analysis of various cooling methods. To effectively imitate the conditions that a server would undergo in a real-world data center, the vehicle can be subjected to a range of various testing scenarios, such as increasing server density, higher temperatures, and varied humidity levels. This enables the evaluation of various cooling methods under a wide range of situations, providing significant insights into their effectiveness and efficiency. The thermal test vehicle used for this study is a ceramic heater of 5x5x3 cm (length x width x height) and a T-type thermocouple is grooved at the center to provide the case temperature as shown in figure 3.1. The bracket holds the TTV base, and the heater assembly as shown, the base holds the heater assembly which resembles a graphical processing unit (GPU) and provides the desired 1000W of heat load (Q) for testing. The cold plate is mounted over the top of this assembly and phase change thermal interface material (TIM) which has conductivity 7 W/m.K is used for the testing purposes.
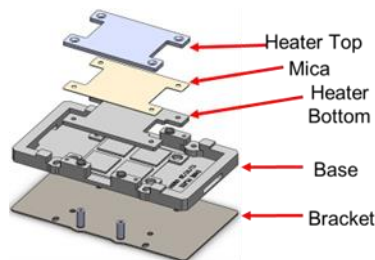

FIGURE 3.1: TTV DESIGN FOR COOLANT TESTING

3.2.1.2   EXPERIMENTAL SETUP

The thermal testing vehicle is built with a closed-loop system that includes a single micro fin channeled cold plate that serves as a direct-to-chip liquid-cooled heat sink. This cold plate is mounted on top of the thermal test vehicle, which serves as a heat source. To evaluate hydraulic and thermal properties, pressure sensors with a range of 0 to 15 psi and t- type thermocouple with a range of -185℃ to +300℃ are mounted in series before and after the cold plate. These pressure sensors have a 0.05% precision, while the t-type thermocouple has a 0.75% accuracy. A stainless-steel reservoir is linked in series to two centrifugal pumps to circulate the fluid throughout the loop. In addition, the coolant's heat is dissipated from it and kept at the required inlet temperature by a flat plate heat exchanger that is connected to a chiller unit. A needle valve is also utilized to control the flow, and a strainer with a 50-micron screen is used to filter out any dust or foreign particles that could harm the micro-channeled fins. Connecting all the sensors to a data-acquisition unit to log the information allows for real-time data acquisition. The thermal testing vehicle's complete design provides for reliable measurement and monitoring of hydraulic and thermal parameters, as well as the capacity to modify and manage coolant flow rate and temperature. High-precision pressure sensors, t-type thermocouples, and flow sensor are used to assure reliable data capture for thermal and hydraulic analyses. Figure 3.2 shows the schematic layout of the experimental setup for the coolant testing. For each coolant testing, the test setup is rebuilt with new hoses and cold plate of same parameters to ensure no cross contamination among different fluids and the test setup is thoroughly cleaned before testing the coolants. The cleaning procedure for the entire test setup is further described in this paper. Figure 3.3 shows the experimental setup built in the lab for the testing.
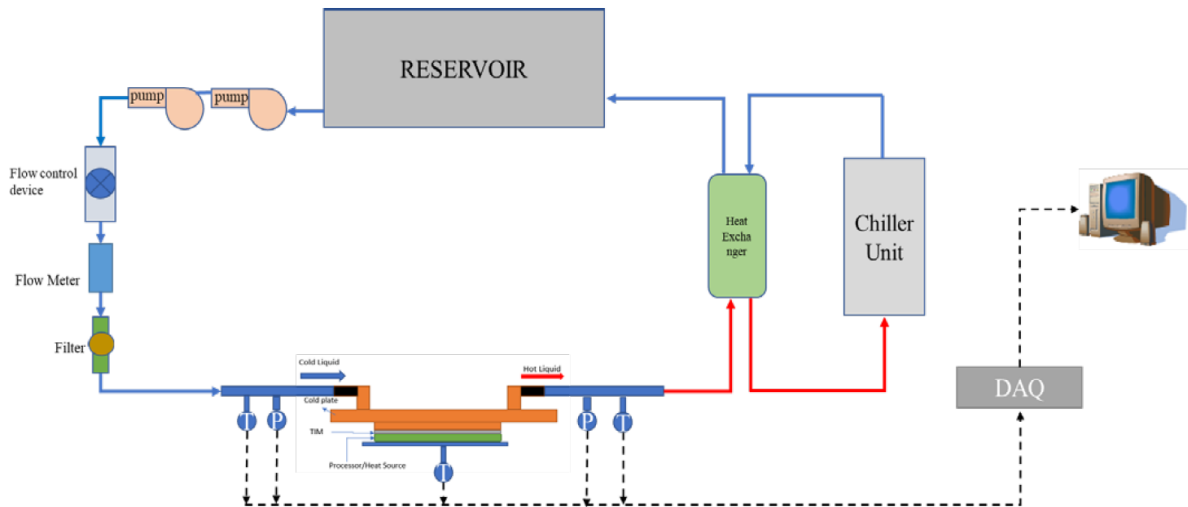

FIGURE 3.2: SCHEMATIC LAYOUT OF THE EXPERIMENTAL SETUP FOR COOLANT'S THERMAL AND HYDRAULIC TESTING
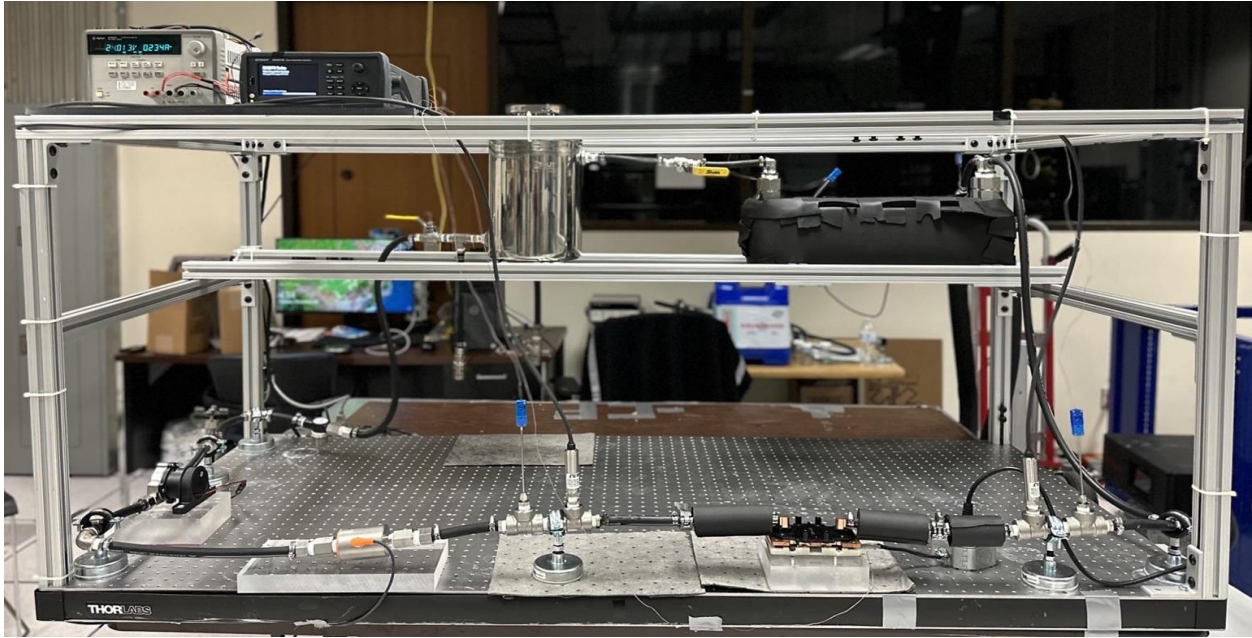
FIGURE 3.3: EXPERIMENTAL SETUP FOR COOLANT'S THERMAL AND HYDRAULIC TESTING

3.2.1.3. **WETTED MATERIAL**

The materials that come in direct contact with the coolant are referred to as wetted materials. The wetted materials include an EPDM rubber hose, stainless steel 316, and Copper C1100. The arrangement guarantees interoperability with the hardware in a real-time data center by utilizing these materials. Cold plates and heat exchangers frequently employ copper Cu C1100 because of its high thermal conductivity. The corrosion resistance and durability of stainless steel 316 make it ideal for usage in moist situations. Rubber EPDM hose is frequently used in fluid transfer applications because it is heat- and chemical-resistant. The fluids specification is closely tied to the wetted material list. Table 3.1 shows the list of wetted materials used.

Material	Details
Copper	CDA1100
Stainless Steel	304, 316 or higher grades
EPDM	Ethylene propylene diene monomer

TABLE 3.1: Acceptable Wetted Materials

3.2.1.4. **UNCERTAINTY ANALYSIS**

Uncertainty analysis is critical in assessing measurement accuracy and reliability for temperature, pressure, and flow sensors. Uncertainty in these sensors can be caused by a variety of variables, including random changes in measurement signals, systematic mistakes in sensor calibration, and environmental influences such as temperature, humidity, and vibration. It is critical to identify and estimate the degree of these uncertainties while undertaking uncertainty analysis. This can be performed using statistical approaches such as standard deviations or mathematical models that characterize sensor behavior and its surroundings. The overall uncertainty associated with the measurement may be estimated and displayed as a confidence

interval by integrating these uncertainties using statistical models. With a particular degree of confidence, this range of values represents the predicted real value of the measured quantity. Uncertainty analysis is critical for guaranteeing measurement reliability and may be applied in scientific, industrial, and regulatory settings. It also allows for the comparison of measurement findings collected from various sensors or measurement systems, as well as the construction of traceability to national or international standards. Table 3.2 displays the parameters of uncertainty that were ascertained through the calibration methodologies. The uncertainty model for the pressure sensor is as follows: C= Pref – PUUC. Where C is the correction factor , Pref is the reference reading and PUUC is the reading from the unit that needs to be calibrated, for the pressure sensor calibration the uncertainty considered is the unit of resolution and repeatability. The resolution of the instrument is considered as the range of square distribution for calculations. Thus, resolution is $\mu UUCres$ is 0.0274 and for any test point, the maximum extend is used in the uncertainty calculation for the repeatability. For this analysis, 3 cycles are performed , thus this value is divided by 1.695. Thus, the total uncertainty contribution for the pressure sensor is ± 2 kPa. For the temperature sensors calibration, the uncertainty associated with the thermal bath is the homogeneity and stability. The stability of the thermal bath is 0.01℃ and the uncertainties associated with the thermocouple units for calibration are the repeatability(μTca), hysteresis (μTch), and due to possible heat conduction ($\mu Tccon$) by the instrument. Approximately 50 measurement readings were taken at each of the calibration temperature and standard deviation was calculated, and the repeatability calculated for μTca 0.002℃. The thermal hysteresis shows $\mu Tch=0.002℃$ and $\mu Tccon$ to be 0.0012 ℃, that was calculated based on the change in temperature when the thermocouples were lifted out of the thermal bath.

Equipment	Uncertainty Values
Flow sensor	0.3%
Pressure sensor	0.25%
T-type thermocouple	± 0.75℃

TABLE 3.2: Uncertainty Analysis

3.2.1.5.   CALIBRATION OF SENSORS

Pressure sensors were calibrated using the Fluke Calibration P5510 Pneumatic Comparison Test Pump, which has a dual pressure/vacuum range of 0 to 300 psi (20 bar) and 0 to 24 inHg (800 mbar). After collecting repeated pressure sensor readings, the slope and gain values were calculated to minimize data variations. The T-type thermocouples were calibrated in a Fluke Calibration 6109A Portable Calibration Bath across a temperature range of 10C to 150C. To reduce disparities between measured and real values, the slope and gain values were adjusted. The magnetic inductive flow sensor was calibrated using a Coriolis mass flow meter at varied flow rates and temperatures. Finally, the measurements were tuned to get the appropriate span. Figure 3.4 shows a pneumatic pressure comparator utilized to calibrate the pressure sensor.

FIGURE 3.4: PNEUMATIC PRESSURE COMPARATOR

3.2.1.6. COOLANT DESCRIPTION

For this study, different coolants from different vendors are used for the testing, the coolants used are propylene glycol with concentrations of 10%, 25%, & 55% and ethylene glycol with concentrations of 10%, 25%, & 55%. These coolants are provided by three different vendors, namely vendor A, C and B. Among propylene and ethylene glycol, treated water is also tested and is provided from vendor D and E.

Ethylene Glycol (EG) is a common antifreeze used in automotive engine coolant; it is also used in applications including process cooling at lower temperatures. Ethylene glycol is colorless, odorless, and completely miscible with water. When inhibited with proper inhibitors it is less corrosive, but still ethylene glycol is toxic and should be handled with care. The quality of water used to make glycol solution is also important, water with low sulphate and chloride concentration (<25 ppm) is recommended. Once the inhibitors are depleted it is necessary that the old glycol is removed. And an inhibited propylene glycol (PG) possesses the same advantages as ethylene glycol of being less corrosive and in addition being non-toxic. [28] Table 3.3, 3.4 & 3.5 shows the different properties of EG and PG coolants from vendors A, B & C respectively. Table 3.6 shows the properties for treated water from vendor D and E respectively.

Vendor A		
Properties	Propylene Glycol	Ethylene Glycol
Appearance	Clear	Clear
pH	N/A	N/A
Melting Point	-60°C	-13°C
Vapor Density	N/A	N/A

Table 3.3: Physical & Chemical Properties for Vendor A

Vendor C		
Properties	Propylene Glycol (10-100%)	Ethylene Glycol (15-100%)
Appearance	Clear	Clear
pH	7.0-11.0	7.0-11.0
Melting Point	-51.1°C	-16.7°C
Vapor Density	2.62	2.14

Table 3.4: Physical & Chemical Properties for Vendor C

Vendor B	
Properties	Propylene Glycol (25%)
Appearance	Greenish Yellow
pH	7.8-8.6
Melting Point	-11.1°C
Vapor Density	Not Available

Table 3.5: Physical & Chemical Properties for Vendor

Treated Water		
Properties	Vendor D	Vendor E
Appearance	Colorless	Colorless
pH	9	8.5-9.0
Boiling Point	100°C	100°C
Freeze Point	0.5°C	0.5°C

Table 3.6: Treated water properties from Vendor D and E

Table 3.7 shows the general properties at 25°C such the thermal conductivity, viscosity, density, and specific heat capacity of the heat transfer fluids used in this study.

General Properties of Heat Transfer Fluid @ 25°C				
Fluid	Specific Heat, Cp (kJ/kg°C)	Density (kg/m^3)	Viscosity (Pa.s)	Thermal Conductivity (W/mK)
EG-10	4.0915	1022.4	0.000843	0.527
EG-25	3.8885	1041.94	0.0015	0.481
EG-55	3.395	1089.28	0.003097	0.368
PG-10	4.103	1015.80	0.0009452	0.508

PG-25	3.9675	1021.52	0.00217	0.474
PG-55	3.465	1042.72	0.006712	0.345
Treated Water	4.187	997.05	0.0008891	0.598

Table 3.7: Properties of Heat transfer Fluids

Table 3.8 shows the different concentrations of propylene glycol and ethylene glycol tested for different vendors and the type of test performed.

Coolant	Concentration (%)	Vendor	Type of Test
Propylene Glycol	10	A, &C	Thermal
	25	A, B &C	Thermal & Reliability
	55	A, & C	Thermal
Ethylene Glycol	10	A, & C	Thermal
	25	A, & C	Thermal
	55	A, & C	Thermal
Treated Water	100	D, & E	Thermal

Table 3.8: Concentration of PG and EG from different vendors

3.2.1.7.   CLEANING PROCESS

The test loop was initially filled with a mixture of DI water and Spectrus NX1106 (<10 ml), an effective antibacterial agent with corrosive capabilities that is useful in concentrations ranging from 0.2 to 0.5 liters/ton. The loop was then drained and cleaned with DI water to remove any remaining cleaning solution residues. Following that, a tiny volume of coolant was injected and cycled through the loop to confirm that no traces of DI water remained that may affect the glycol concentration. After the system had been completely emptied, coolant was injected, and the reservoir was filled to the desired level. High flow rates were then employed to circulate the coolant around the loop and eliminate any air bubbles that might influence the thermal and hydraulic performance of the cold plate. Following the completion of the testing, the coolant was drained, and the cleaning procedure was repeated. To ensure that the testing results were consistent and free of cross-contamination, a fresh cold plate with the same design was used for each kind of coolant, and the EPDM hoses were replaced with new ones.

3.2.1.8.   EXPERIMENTAL PROCEDURE

The experimental setup is constructed on a benchtop, ensuring that the loop is free from any contamination and air bubbles after following the cleaning procedure. Power is supplied to the TTV of 1000W. Before commencing the testing, the thermal interface material should settle between the heater and cold plate for maximum heat transfer. The flow rate is initially limited to a minimum at a high inlet temperature (45°C). Once the TIM is adequately set, the flow rate and inlet temperature are adjusted to the desired condition. After stable readings are obtained from the sensors, the data is logged using the data acquisition device. The study employs ASHRAE test conditions of 17°C, 25°C, 35 °C, and 45 °C, with flow rates maintained at

0.5lpm, 1lpm, 1.5lpm, and 2lpm for all four inlet temperatures. The entire experiment consists of 16 different scenarios performed on a single coolant, and each set of experiments is conducted for thirty minutes. The recorded inlet and outlet pressure and temperature values are then utilized to calculate the cold plate's thermal and hydraulic performance.

3.3. RESULTS AND DISCUSSION

The results and discussion section are broadly divided into two parts thermal & hydraulic testing and second is reliability of the secondary coolants. Cold plate-based coolants are tested at cold plate level for their thermal and hydraulic comparison using the experimental setup as shown in the previous section above. Further reliability of coolants was tested using ASTM D1384 apparatus which is the test technique for determining the corrosive effects of various coolants under stress.

3.3.1. THERMAL AND HYDRAULIC EXPERIMENTS

The thermal and hydraulic testing of cold plate-based coolants was performed using bench top setup as shown in the figure 3.3. Single cold plate with TTV is used to characterize the coolants. Pump pushes the coolant from the reservoir to the cold plate extract the heat and reject it to the liquid-to-liquid heat exchanger before going back to the reservoir. The cold plate was instrumented with T type thermocouple and pressure sensor to the inlet and outlet of it. Before starting any experimental test, the setup was cleaned following the process as explained above. All the different coolant experiments were performed at 1000 watts or 40 watts/cm² power, coolant supply temperature was varied from 17 °C to 45 °C and flow rate was varied from 0.5 lpm to 2 lpm. The coolants tested for these experiments were water-based coolants like PG with 10, 25 and 55% concentration, EG with 10, 25 and 55% concentration and treated water from multiple vendors.

3.3.1.1. THERMAL PERFORMANCE OF COLD PLATE BASED WATER COOLANTS

To measure the thermal performance of the coolant thermal resistance was calculated using the formula shown in below equation (1).

$$R_{th} = \frac{(T_{base} - T_{inlet})}{Q} \ (°C/W)$$

(1)

Here, T_{base} is the base temperature measured from the thermocouple grooved on the heater of the TTV, and T_{inlet} is the fluid's inlet temperature, and Q is the heat load provided for testing. The graph shown below from figure 3.5-3.7 shows the thermal performance of the different concentrations of propylene glycol in the water. Figure 3.5 shows the PG-10 thermal resistance at different flow rates. At 0.5 lpm for vendor A coolant R_{th} was 0.04239 °C/W and for vendor C it was 0.04119 °C/W. At 2 lpm flow rate R_{th} for vendor A and C was dropped to 0.0226 and 0.0218 °C/W, variation in thermal resistance value for two vendor lies within the error bar. Third bar show the average reading of the PG-10 obtained, which is 0.0417 °C/W at 0.5 lpm and 0.0222 °C/W at 2 lpm flow rate.
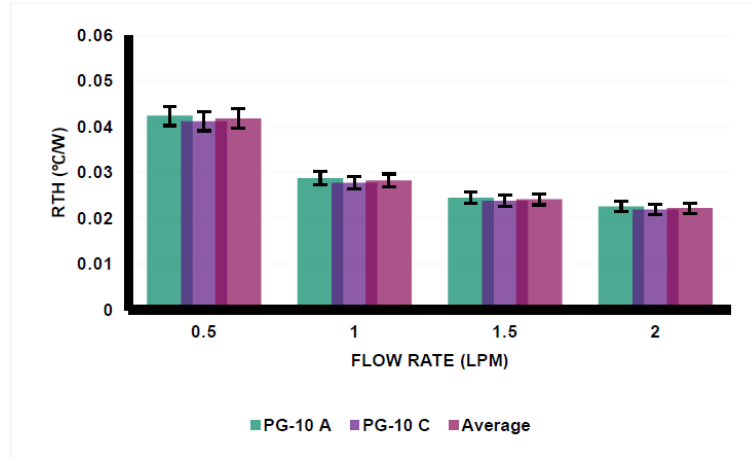
FIGURE 3.5: THERMAL RESISTANCE VS FLOW RATE FOR PG 10

Figure 3.6 shows the PG-25 thermal resistance. For PG-25 three vendor coolants were tested, at 0.5 lpm for vendor A, B and C coolant R_{th} was observed 0.0444 °C/W, 0.04202 °C/W and 0.04315 °C/W respectively. At 2 lpm R_{th} drops to 0.02419, 0.02214 and 0.02321 °C/W respectively. The average value of R_{th} was calculated as 0.04319 °C/W at 0.5 lpm and 0.02318°C/W at 2lpm. Overall, for PG-25 vendor B shows better thermal resistance than vendor A and C but it mostly lies within the error bars.
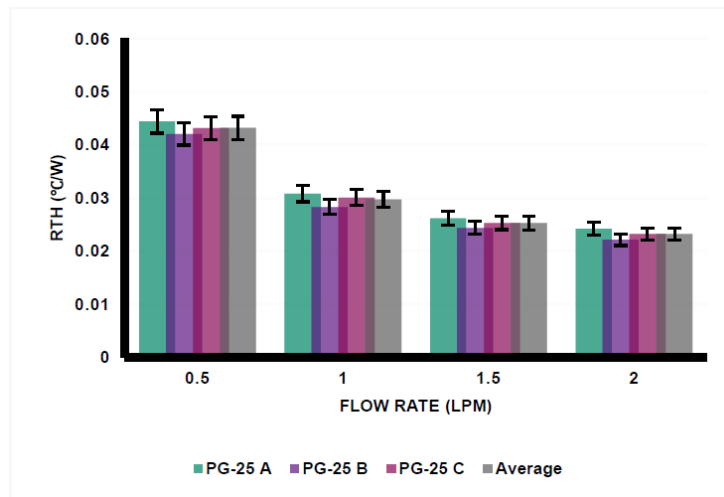

FIGURE 3.6: THERMAL RESISTANCE VS FLOW RATE FOR PG- 25

Similarly, Figure 3.7 shows the thermal resistance of the PG-55 acquired from the two different vendors. PG-55 R_{th} was observed around 0.0493 °C/W and 0.0501 °C/W for vendor A and C at 0.5 lpm and it dropped to 0.02707 °C/W and 0.0284 °C/W at 2 lpm.
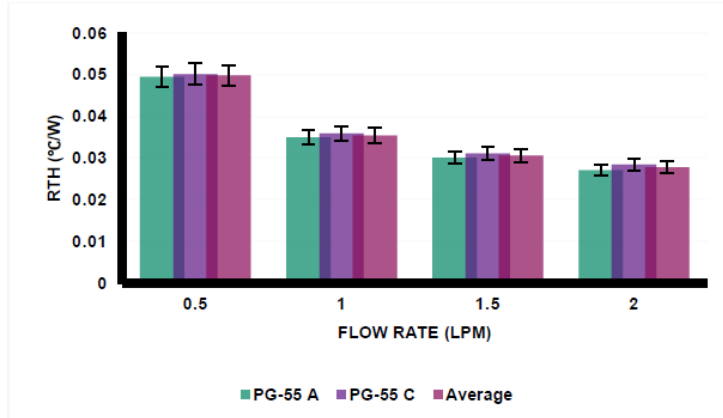
15

FIGURE 3.7: THERMAL RESISTANCE VS FLOW RATE FOR PG- 55

Overall PG-55 has shown the highest thermal resistance when compared to PG-10 and PG-25 because of its degraded thermal properties as discussed in the material and method section. PG-55 thermal performance was on an average 18.823% lower with respect to PG-25 and PG-10 show the on an average thermal performance of 4.12% higher than the PG- 25.

Though PG-10 performance is better than the PG-25 and PG-55 but it is not used in the industry because of bio growth when used for long time [31]. Whereas coolants with PG concentration of more than 20% are considered biologically stable. PG-25 and PG-55 both can be used in the data centers, but PG-25 is preferred over PG-55 because of the higher thermal properties as shown.

The graph shown below from figure 3.8-3.10 shows the thermal performance of the different concentration of Ethylene glycol in the water. Figure 3.8 shows the EG-10 thermal resistance at different flow rates. At 0.5 lpm for vendor A and C coolant R_{th} was 0.04013 °C/W and 0.0411 °C/W. At 2 lpm flow rate R_{th} for vendor A and C was dropped to 0.0207 and 0.02111 °C/W respectively. The average reading of the EG-10 was obtained as 0.0406 °C/W at 0.5 lpm and 0.0209 °C/W at 2 lpm flow rate. Figure 3.9 shows the EG-25 thermal resistance. At 0.5 lpm for vendor A and C coolant R_{th} was observed 0.0418°C/W and 0.0422 °C/W respectively. At 2 lpm R_{th} drops to 0.0223 and 0.02309 °C/W respectively. The average value of R_{th} was calculated as 0.042 °C/W at 0.5 lpm and 0.0223 °C/W at 2lpm. Figure 3.10 shows the thermal resistance of the EG-55 acquired from the two different vendors. EG-55 R_{th} was observed around 0.047 °C/W and 0.046 °C/W for vendor A and C at 0.5 lpm and it dropped to 0.0254 °C/W and 0.026 °C/W at 2 lpm.
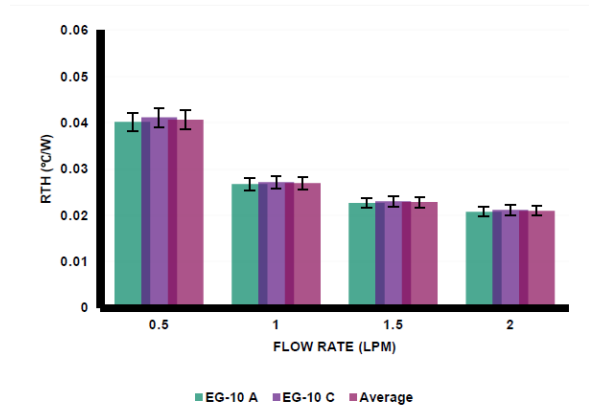
16

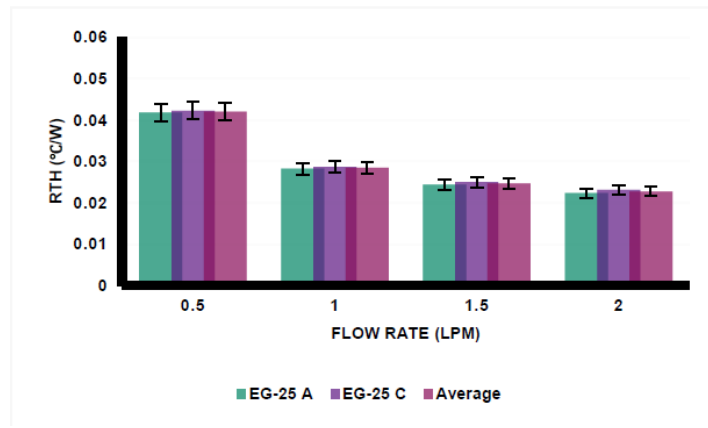FIGURE 3.8: THERMAL RESISTANCE VS FLOW RATE FOR EG10

FIGURE 3.9: THERMAL RESISTANCE VS FLOW RATE FOR EG25
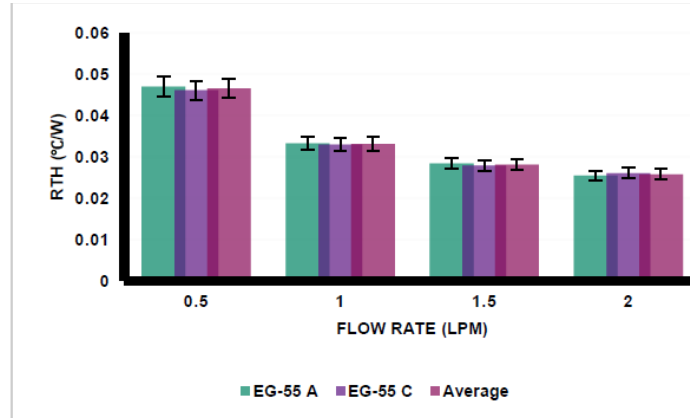
FIGURE 3.10: THERMAL RESISTANCE VS FLOW RATE FOR EG-55

Like PG-55 case, EG-55 has shown the highest thermal resistance when compared to EG-10 and EG-25 because of its degraded thermal properties as discussed in the material and method section. EG-55 thermal performance was on an average 10.48% lower with respect to PG-25, EG-25 show the on an average thermal performance of 2.77% higher than the PG25 and EG-10 show 8.68% higher thermal performance than PG-25. When comparing water-based coolants with ethylene glycol and propylene glycol bases, it is evident that ethylene glycol exhibits superior thermal and hydraulic performance. This can be attributed to its enhanced

thermal properties, including higher thermal conductivity and lower viscosity, in comparison to propylene glycol-based water coolants, despite both coolants having similar thermal mass. As mentioned above in coolant description, ethylene glycol being toxic in nature is not used in data center industry.

The treated water was also tested for this study and the results of it are shown in figure 3.11 below. Two vendors treated water were tested and the result obtained from them are quite similar. Treated water has shown one of the lowest thermal resistances. The average value of R_{th} at 0.5 lpm and 2 lpm was obtained as 0.03906 °C/W and 0.0189 °CW respectively.

FIGURE 3.11: THERMAL RESISTANCE VS FLOW RATE FOR TREATED WATER

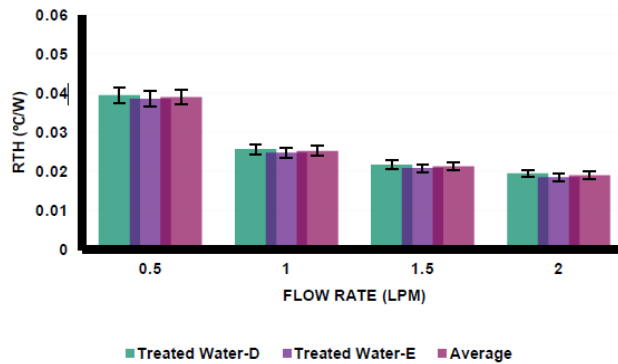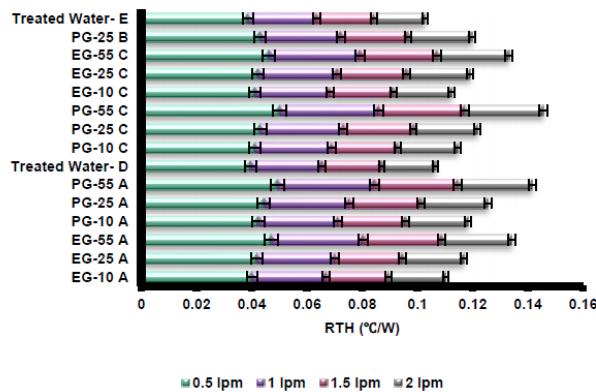FIGURE 3.12: CUMMULATIVE THERMAL RESISTANCE VALUE FOR ALL COOLANTS

Figure 3.12 shows the cumulative thermal resistance value of all the coolants tested. It shows that treated waters have the lowest thermal resistance followed by Ethylene based coolants and followed by propylene-based coolants.
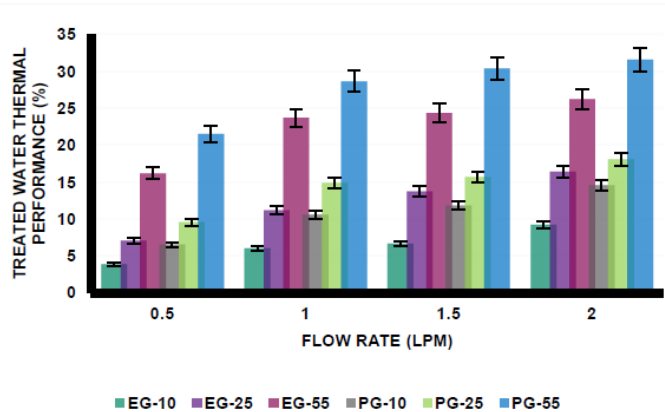
18

FIGURE 3.13**:** TREATED WATER PERFORMANCE COMPARED WITH OTHER GLYCOL COOLANTS

Figure 3.13 shows the treated water performance compared to other glycol-based coolants. The thermal performance of the treated water increases when compared with different concentration of glycol at varying flow rates. The thermal performance of treated water increases as the flow rate increases and compared with the increasing concentration of glycol. The highest thermal performance of treated water is with respect to PG-55. Treated water shows 21.49% higher thermal performance at 0.5 lpm and 31.57% higher thermal performance at 2 lpm. The lowest thermal performance of treated water was with respect to EG-10, treated water thermal performance was just 3.87% higher at 0.5 lpm and 9.22% higher at 2 lpm. As compared to PG-25, which is a widely used coolant in liquid cooled data centers. Treated water performance was 9.57% higher at 0.5 lpm and 18.07% higher at 2 lpm. This higher performance of treated water will help to save pumping power at data center level. This has been discussed in the coming hydraulic testing results.

3.3.2 HYDRAULIC PERFORMANCE OF COLD PLATE BASED WATER COOLANTS

Liquid cooling using cold plates is an effective method for dissipating heat from electronic components. However, the pressure drop in the liquid cooling system can have a significant impact on its performance. In this study, we measured the pressure drop for different coolants at different flow rates of 0.5 lpm, 1 lpm, 1.5 lpm, and 2 lpm. The coolants used were propylene glycol (PG), ethylene glycol (EG) different concentrations (10, 25 and 55%) and treated water at four different supply temperatures (17°C, 25°C, 35°C and 45°C). The graph shown above from figure 3.14-3.17 shows the pressure drop of different coolants tested at different supply temperature and flow rate. Figure 3.14 shows the pressure drops of the all the coolants tested at 17 °C supply temperature, as expected treated water shows the lowest pressure drop as compared to other glycol-based coolants. Pressure drop of Treated water was observed to be 0.071 psi at 0.5 lpm and 0.945 psi at 2 lpm flow rate. The reason for the low pressure drops of treated water compared to other coolants is because of its lowest viscosity as shown in section 2.1.6. PG-55 has the

highest pressure drop of 0.278 psi at 0.5 lpm and 2.35 psi at 2 lpm because of its highest viscosity. Similar results were obtained for the other supply coolant temperature as seen in figures 3.15-3.17. Lowest pressure drops for all the coolants were obtained at 45 °C supplied coolant temperature because for all the coolant viscosity is the function of temperature and it decreases with increase in temperature. Pressure drops of PG- 55 at 45 °C were 0.142 psi and 1.26 psi at 0.5. lpm and 2 lpm respectively, whereas for treat ed water it was 0.0204 psi and 0.685 psi at 0.5 lpm and 2 lpm respectively. The pressure drop in a liquid cooling system can be affected by numerous factors such as the flow rate, coolant type, coolant temperature, and the design of the cooling system. The results of this study show that the pressure drop in a cold plate-based liquid cooling system increases with increasing flow rate for all coolants tested. Moreover, the pressure drop varies depending on the coolant type and temperature. Treated water showed the lowest pressure drop, which could make it a preferred coolant for cold plate-based liquid cooling systems where low-pressure drop is desirable.
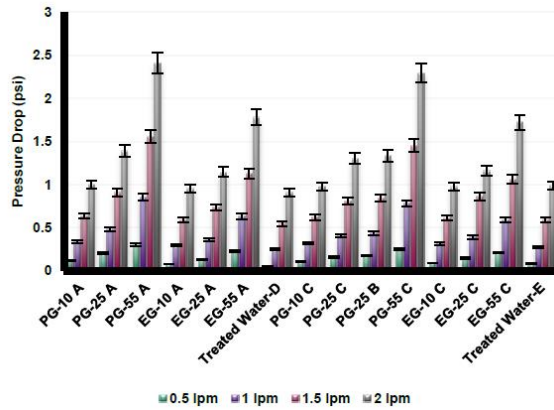

FIGURE 3.14: PRESSURE DROP FOR DIFFERENT COOLANTS TESTED AT DIFFERENT FLOW RATES AT 17 °C
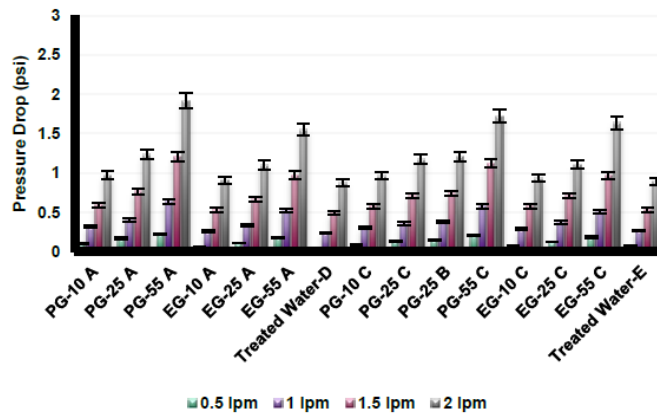

FIGURE 3.15: PRESSURE DROP FOR DIFFERENT COOLANTS TESTED AT DIFFERENT FLOW RATES AT 25 °C
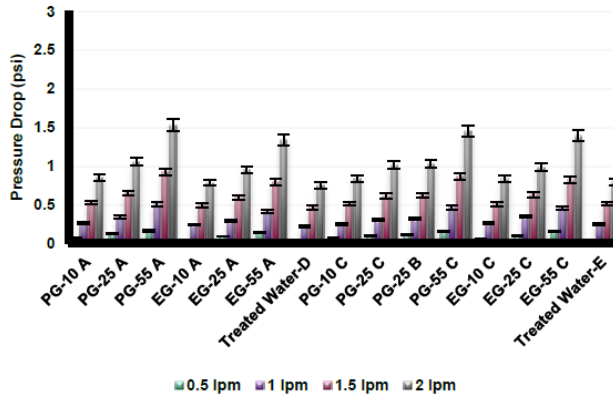
FIGURE 3.16: PRESSURE DROP FOR DIFFERENT COOLANTS TESTED AT DIFFERENT FLOW RATES AT 35 °C
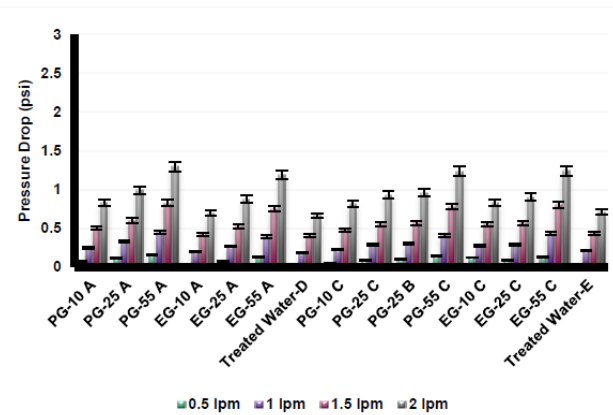
FIGURE 3.17: PRESSURE DROP FOR DIFFERENT COOLANTS TESTED AT DIFFERENT FLOW RATES AT 45 °C

3.3.3 CONCLUSION

A variety of single-phase liquid coolants are available in the market, including propylene glycol (PG), ethylene glycol (EG), DI water, treated water, and nanofluids. Different manufacturers produce these coolants, incorporating a range of inhibitors and chemicals to improve their long-term effectiveness, prevent the growth of organisms, and offer corrosion protection. Nonetheless, the thermal performance of these coolants can be influenced by the additives used, even when the base coolant is identical. This study seeks to compare these coolant varieties and assess the performance of the same coolant obtained from different vendors. For the experimentation, a benchtop setup centered around a single cold plate was constructed. The setup included essential components such as a thermal test vehicle (TTV), pump, reservoir, flow sensor, pressure sensors, thermocouple, data acquisition units, and heat exchanger. To ensure accuracy, each coolant underwent testing on its dedicated cold plate, and meticulous cleaning procedures were performed before every experiment. Consistent boundary conditions were maintained throughout the experiments, with a TTV power of 1000

21

watts and varying coolant flow rates (ranging from 0.5 lpm to 2 lpm) as well as supply coolant temperatures (17°C, 25°C, 35°C, and 45°C) to simulate warm water cooling. This allowed for the acquisition of graphs depicting thermal resistance (R_{th}) versus flow rate and pressure drop (ΔP) versus flow rate for each coolant. Additionally, the effect of different supply coolant temperatures on pressure drop was thoroughly analyzed.

The overview of the paper touches on the following aspects.

1. For the thermal and hydraulic testing of different coolants, a single cold plate benchtop setup was developed. Exacting standards of meticulous cleanliness were diligently upheld between the sequential experiments involving distinct coolants.

2. Upon analysis of the thermal and hydraulic testing results, it was observed that despite the utilization of diverse inhibitors and chemicals by different vendors to deter bio growth and corrosion within the identical base fluid, the thermal and hydraulic performance exhibited remarkable similarity. The disparities observed fell well within the acceptable margin of error, approximately 5%.

3. When comparing water-based coolants with ethylene glycol and propylene glycol bases, it is evident that ethylene glycol exhibits superior thermal and hydraulic performance. This can be attributed to its enhanced thermal properties, including higher thermal conductivity and lower viscosity, in comparison to propylene glycol-based water coolants, despite both coolants having similar thermal mass.

4. Among all the coolants tested, treated water exhibited the most exceptional thermal performance. The average thermal resistance of treated water at a flow rate of 0.5 liters per minute was approximately 0.039
°C/W, while at a flow rate of 2 liters per minute, it was approximately 0.0189 °C/W because of its better thermal properties.

5. This study aimed to assess the pressure drop characteristics of various coolants at different flow rates, namely 0.5 lpm, 1 lpm, 1.5 lpm, and 2 lpm. The coolants investigated in this study included propylene glycol (PG), ethylene glycol (EG) at different concentrations, and treated water. Additionally, the coolants were subjected to four distinct supply temperatures, namely 17°C, 25°C, 35°C, and 45°C. Treated water showed the lowest pressure drop outperforming other glycol-based coolants.

Chapter 4

METHODOLOGY TO CHARACTERIZE ROW MANIFOLDS FOR HIGH POWER DIRECT TO CHIP LIQUID COOLING DATA CENTERS

4.1 ABSTRACT

Demand is growing for the dense and high-performing IT computing capacity to support artificial intelligence, deep learning, machine learning, autonomous cars, the Internet of things, etc. This led to an unprecedented growth in transistor density for high-end CPUs and GPUs, creating thermal design power (TDP) of even more than 700 watts for some of the NVIDIA existing GPUs. Cooling these high TDP chips with air cooling comes with a cost of the higher form factor of servers and noise produced by server fans close to the permissible limit. To overcome these issues for high TDP chips advanced cooling technologies, need to be investigated. Liquid cooling is becoming more mainstream to overcome the some of challenges mentioned above. Direct-to-chip cold plate-based liquid cooling is highly efficient and becoming more reliable as the advancement in technology is taking place. Several components are used in the liquid-cooled data centers for the deployment of cold plate based direct to chip liquid cooling like cooling loops, rack manifolds, CDUs, row manifolds, quick disconnects, flow control valves, etc. Row manifolds used in liquid cooling are used to distribute secondary coolant to the rack manifolds. Characterizing these row manifolds to understand the pressure drops and flow distribution for better data center design and energy efficiency is important. In this paper, the methodology is developed to characterize the row manifolds. Water-based coolant Propylene glycol 25% was used as the coolant for the experiments and experiments were conducted at 21 °C coolant supply temperature. Highly calibrated Pressure sensors were used at the supply port of the row manifolds and the inlet-outlet of the main hose to measure the supply pressure of ports and pressure drop across the row manifold respectively. Similarly, ultrasonic flow sensors were used to measure the flow rate at each supply port and the main entrance of the row manifold. Two, six-port row manifolds' P-Q curves were generated, and the value of supply pressure and the flow rate were measured at each port. The results obtained from the experiments were validated by a technique called Flow Network Modeling (FNM). FNM is a 1-D simulation suited for the analysis of flow distribution in liquid cooling systems. The FNM technique uses the overall flow and thermal characteristics to represent the behavior of individual components. Therefore, the solution of conservation equations over the network enables efficient prediction of the flow rates, pressures, and temperatures in a complete liquid- cooling system.

4.2 EXPERIMENTAL SETUP AND PROCEDURE

The experimental setup consists of eight 52U racks, two- row manifolds of six ports each, eight rack manifolds, a Coolant distribution unit, and flow, temperature, and pressure sensors to measure data as shown in figure 4.1 below. The CDU used in this study was 450 kW, which can provide a maximum flow rate of 500 lpm at an external pressure drop of 3.4 bar. The hose connecting the CDU with the Y connectors were having pressure sensor to measure pressure drop across the row manifold. The hoses connecting row manifolds ports with rack manifolds have pressure sensors and flow sensors to measure the supply, return pressure, and flow rate, respectively. The coolant used in this study was propylene glycol 25% (PG-25). The coolant was maintained at a set temperature by the CDU, this coolant then passes through the Y connectors in the setup and is distributed among two supply row manifolds. Supply row manifolds then distribute coolant to supply rack manifolds and row manifolds are connected to rack manifolds with the help of Eaton valve FD-83. From the supply rack, manifold coolant is then delivered to the cooling loops, where coolant captures heat from the IT and follows the path back to the CDU using the return rack manifold, row manifold, etc.

This paper focuses on the hydraulic characterization of row manifolds. For the experiments and characterizing the row manifold, ports of row manifolds were short-circuited using FD 83 valves. Out of 6 ports as shown in figure 4.2 below only 4 ports on the row manifolds were considered for this experiment, the first two and last two ports. Out of two-row manifolds (one of copper and another one was steel) in parallel, one row manifold was kept open and allowed the coolant to pass through it at a time while another one was kept closed. The row manifolds were characterized at 21 °C inlet coolant temperature and the flow rate of the coolant varied from 40 to 165 lpm. During the experiment pressure drop across the row manifold, and each port supply pressure and the flow rate were measured.
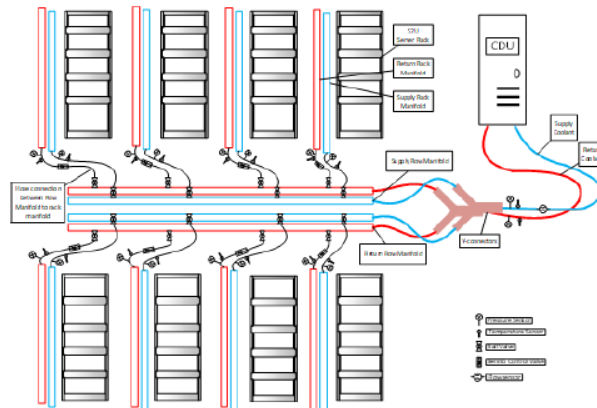

FIGURE 4.1: EXPERIMENTAL PROCEDURE

FIGURE 4.2: ROW MANIFOLD

4.3 SENSOR CALIBRATION

In the experiments, pressure sensors and flow sensors were used. Pressure sensors used were GP-M010 and calibrated using Fluke P5510-2M Pneumatic Comparison Test Pump as shown in the figure below. On the left side of the test equipment was the GP-M010 pressure sensor and on the right side, the reference pressure gauge was mounted. To increase the pressure in the test rig a hand pump was used. The error in the reading of the sensor and the reference gauge was recorded for error analysis. Similarly, the Keyence clamp-on microflow sensors (Keyence FDQ-32C) were calibrated with a Coriolis flowmeter. The K- type thermocouples used to measure the fluid temperature were calibrated using a Fluke 7109A portable calibration bath between a temperature of 0-100°C using a two-point calibration method as shown in Figure. Table 4.1 shown below shows the details of the sensors used in this study. It was observed that the pressure sensors were very precise after factory calibration and did not need additional calibration. A two-point calibration method was used for the thermocouples by calculating the error in the temperature reading. The calibration equation obtained was directly used as input in the DAQ software as gain and offset values. To calibrate the ultrasonic flow sensors, a calibrated Electromagnetic flow sensor was used by placing the flow sensor in the same closed loop along with the Electromagnetic flow meter. Table 4.2 shows the error calculation quantified from the calibration process for pressure sensors, temperature sensors, and flow sensors.
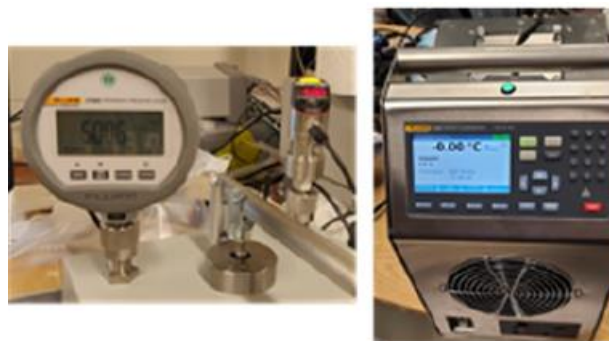

FIGURE 4.3: Fluke P5510-2M Pneumatic Comparison Test Pump and Fluke 7109A portable calibration bath

Sensor	Operating Voltage/current (mA)	Range of measurement	Accuracy
Keyence FDQ-32C	20V – 30V	0.02L/min -20L/min	+0.003ml/min
Keyence Pressure sensors	4-20	0-1000 kPa	+ 0.25%
K – Type Thermocouple	-	0 – 400 ˚C	+ 0.75%

Table 4.1: Details of Sensor Measurement range, accuracy and operating voltages

Reference Guage (KPa)	GP-M010 pressure sensors (KPa)	% Error
150.3	150	0.2
200.2	200	0.1
300.6	300	0.2
400.5	400	0.124
500.6	500	0.12
Reference Temperature (°C)	Measured Temperature (°C)	% Error
10	9.8	2
90	89.3	0.8
Reference Flow Rate at Electromagnetic Sensor (lpm)	Measured Flow Rate at Sensor (lpm)	% Error
10	10.3	3
20	21	5
40	41.3	3.2
50	51.5	3

Table 4.2: Percentage of error during Calibration

4.4 RESULTS AND DISCUSSION

As explained in the experimental setup and procedure section, two-row manifolds were characterized in this study but the results of the one-row manifold are discussed below because of the similarities in the results. The results in this section are divided into two parts, in the first part experimental results will be discussed and in the later part, experimental results will be compared with 1-D flow network simulation results.

In the first set of experiments copper, material-based row manifold was characterized. The flow rate varied from 40 lpm to 167 lpm with a coolant supply temperature of 21 °C. Figure 4.4 shown below shows the flow rate going to the entire row manifold and each individual port. When the system flow rate was around 166.2 lpm the flow rate going to each individual port was around 41.2 lpm, where the maximum difference between the two ports' flow rate was 0.66 lpm, which lies in the range of flow sensor accuracy. Similarly, when the low flow rate of 40 lpm passed through the system, the flow rate going to each individual port was around 9.8 lpm, with the

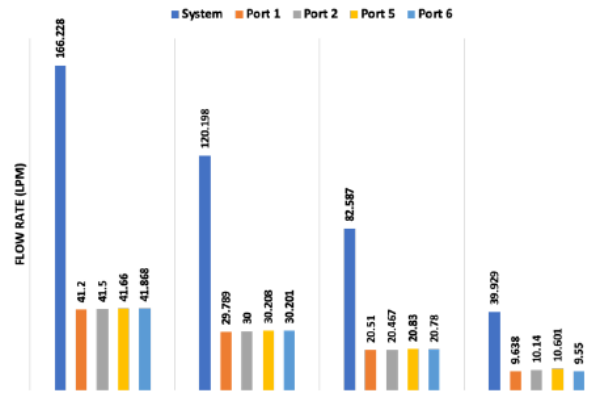maximum difference in flow rate between the two ports being 1 lpm.

FIGURE 4.4: GRAPH SHOWING COPPER ROW MANIFOLD FLOW RATE AND FLOW RATE IN EACH ROW MANIFOLD PORT

The graph shown below in figure 4.5 shows the copper row manifold pressure drop vs flow rate graph. The row manifold had shown a pressure drop of negligible at the flow rate of 40 lpm and of 4.5 psi at the flow rate of 166 lpm. Figure 4.6 shows the supply pressure at the inlet of each port of the row manifold, the average supply pressure at 40 lpm is 15.5 psi and at 166 lpm was 19.2 psi. Though each port shows some variation in the supply pressure at each port, but it was between the pressure sensors' accuracy range.
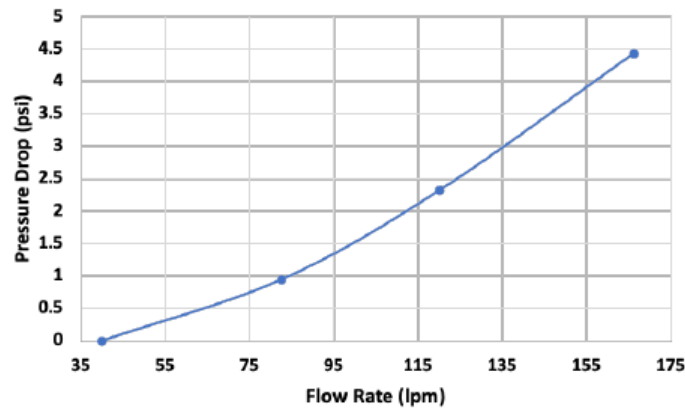

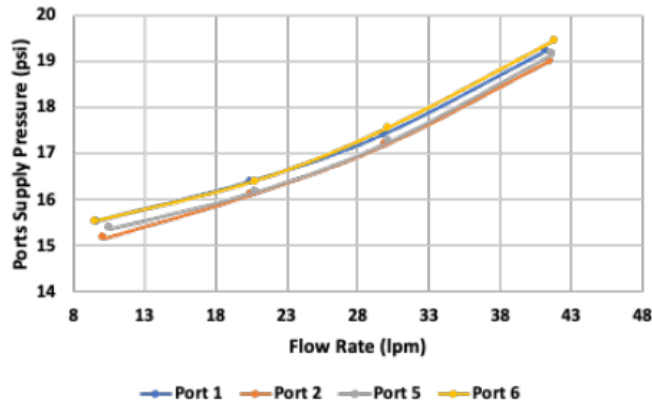FIGURE 4.5: COPPER ROW MANIFOLD PRESSURE DROP VS FLOW RATE

FIGURE 4.6: COPPER ROW MANIFOLD INDIVIDUAL PORT SUPPLY PRESSURE

4.5 CONCLUSION

Given the absence of pertinent literature on row manifolds within liquid-cooled data centers, a unique methodology was devised to systematically characterize these components. The experimentation involved the generation of P-Q curves for six-port row manifolds. At each port, the supply pressure and flow rate were meticulously measured, revealing a remarkably consistent flow rate across all ports. The results indicated a pressure drop of 4.4 PSI at approximately 160 liters per minute (lpm), while negligible pressure drop was observed at the lower flow rate of 40 lpm. The validity and accuracy of these findings were subsequently confirmed through the use of Flow Network Model (FNM) simulations, providing a robust and reliable validation of the developed methodology and its outcomes. This innovative approach contributes valuable insights into the fluid dynamics and performance characteristics of row manifolds, filling a notable gap in the existing body of literature related to liquid-cooled data centers.

Chapter 5

Liquid Cooling Data logging and analysis application

5.1 Introduction

LabVIEW is a visual programming language known for its graphical representation of code. It stands out as a modular platform that readily accommodates expansion through the incorporation of diverse add-ons and libraries. Notably, LabVIEW exhibits a remarkable capability to seamlessly interface with an extensive array of hardware devices, including sensors, data acquisition systems (DAQs), and various instruments.

One of LabVIEW's strengths lies in its prowess as a robust tool for tasks such as data analysis, signal processing, and data visualization. Its graphical nature simplifies complex programming tasks, making it particularly advantageous for users in fields that involve extensive data manipulation and interpretation.

In terms of system architecture, the envisioned software system is crafted using LabVIEW, wherein modules are intricately woven together for tasks encompassing data collection, processing, analysis, and visualization. The architectural blueprint includes components dedicated to both real-time data monitoring and the in-depth scrutiny of historical data. This highlights LabVIEW's role as a comprehensive solution for building sophisticated systems that seamlessly integrate various functionalities crucial for effective and efficient data-driven applications.

5.2 Scope of the work

This thesis project entails the design and implementation of a Liquid Cooling Data Logging and Analysis application using LabVIEW, with the goal of advancing the monitoring and management of liquid-cooled data centers. The project's primary objectives include creating a user-friendly LabVIEW interface for real-time data visualization, implementing statistical analysis algorithms for post-experiment reporting, establishing robust data storage mechanisms, and developing automation features for streamlined testing procedures. The methodology involves graphical programming in LabVIEW, integration of data acquisition modules, and a modular design for scalability. The anticipated deliverables include a LabVIEW application with live data monitoring, automated test scripts, statistical analysis reports, and functionality for storing and retrieving historical experiment data. Ultimately, the thesis aims to contribute to the successful and safe commissioning of liquid-cooled data centers through the application of this comprehensive LabVIEW solution.

5.3 Instrumentation

The workstation's instrumentation setup involved a diverse array of devices connected through different communication interfaces, as outlined in the corresponding table. To facilitate data acquisition and integration into the system, instruments such as the Pressure Sensor, Flow Sensor, T-Type Thermocouples, and 10K Thermistors were interfaced with the workstation through

dedicated DAQ units. The connectivity between these instruments and the workstation was established using USB connections.

In a parallel configuration, devices like the CDU (Control and Display Unit) and Belimo Valves utilized the Ethernet communication protocol. These devices were connected to a LANHUB, forming a network infrastructure. The LANHUB, acting as an intermediary, was then linked to the workstation via a LAN cable. This configuration allowed for efficient communication and control between the CDU, Belimo Valves, and the central workstation.

Moreover, the Power Supply Units were integrated into the system, employing Ethernet communication as well. These units were directly connected to the workstation using Ethernet cables, ensuring a reliable and efficient connection for power supply management.

For a comprehensive understanding of the physical setup, the provided figure 5.1 visually illustrates the interconnections among the various instruments, DAQ units, LANHUB, and the workstation. This elaborate integration of instruments through distinct communication interfaces forms a robust and well-organized system for data acquisition, control, and analysis within the workstation environment.

Device	Type of connection to workstation
DAQ 34970A	Serial USB connection
CDU	Ethernet connection (LAN cable)
Belimo Valve	Ethernet connection (LAN cable)
PSU	Ethernet connection (LAN cable)

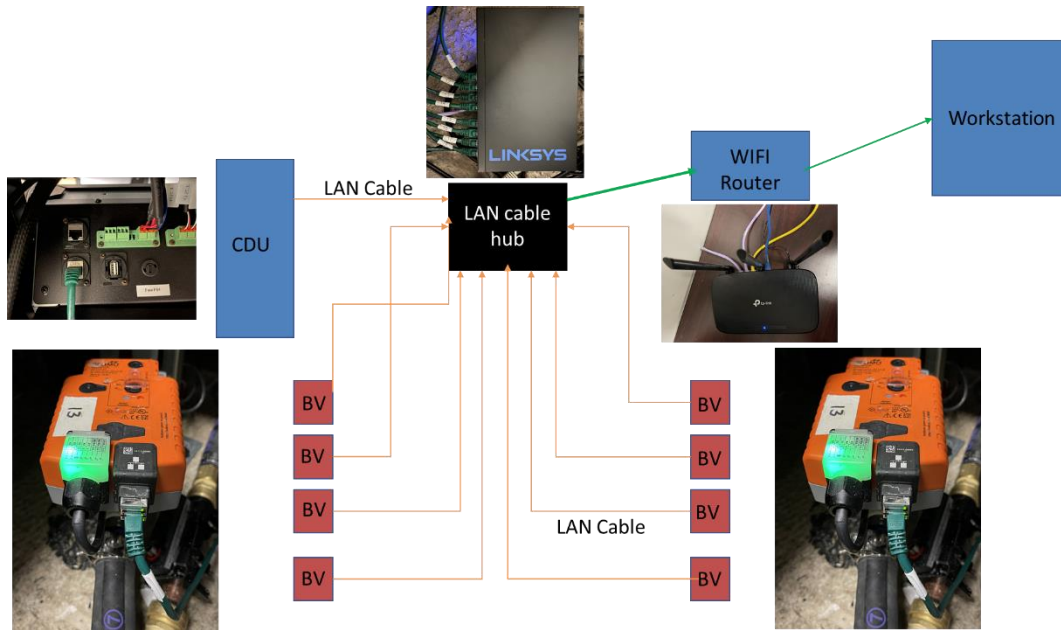Table 5.1 device communication protocol

FIGURE 5.1: DEPICTS THE VISUAL REPRESENTATION OF CONNECTED DEVICES

5.4 Results and Discussions

The front page of the developed software serves as the central hub for user interaction, featuring a well-organized interface with distinct tabs that streamline the user experience. Among the prominent tabs are "Connect/Disconnect Devices," providing a seamless way to establish and terminate connections with hardware components, and "View System," offering an overview of the overall system status. The "View Plots" tab allows users to visualize real-time experimental data through dynamic plots, enhancing the monitoring capabilities of the application. Furthermore, dedicated tabs such as "View Belimos" provide specific insights into the status and performance of Belimo valves. The "Settings" tab enables users to configure essential parameters, while "System Configurations" centralizes overarching settings for the application. Lastly, the "Device Status" tab presents a comprehensive snapshot of the operational status of connected devices. This intelligently designed front page serves as an intuitive control center, empowering users to navigate through various functionalities effortlessly and facilitating a holistic understanding of the system's operations. The inclusion of these tabs on the front page underscores the software's user-centric design, ensuring accessibility and functionality for a diverse range of tasks within the realm of liquid cooling experimentation and monitoring.
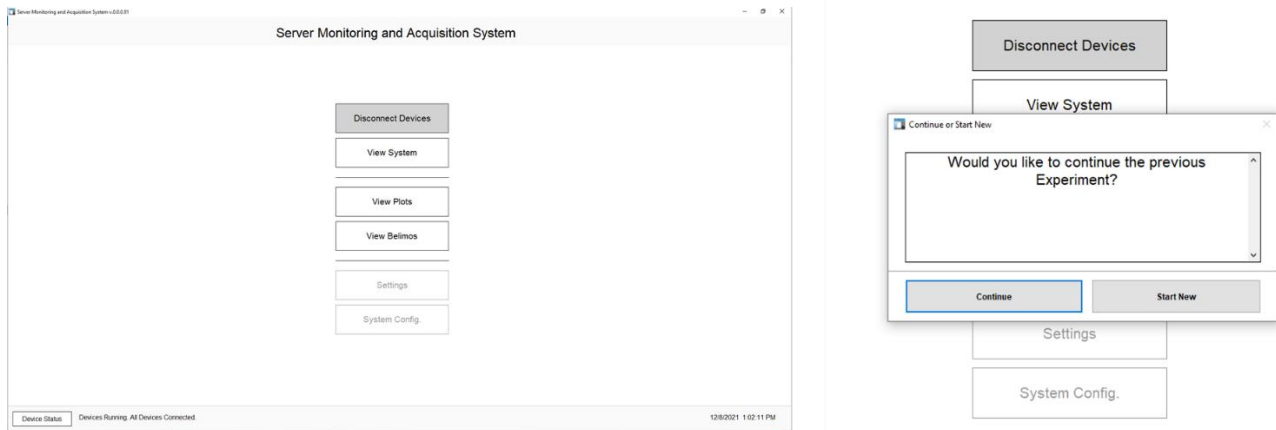
FIGURE 5.2: Front page of the application

The Settings tab within the user interface plays a pivotal role in configuring crucial parameters for the efficient operation of the developed system. Within this tab, users have the capability to define various settings, including the DAQ port, CDU's, and Belimo valve's IP addresses, as well as the serial port associated with the power supply. Additionally, the window provides a dedicated space for the configuration of DAQ channels, allowing for precise customization based on experimental requirements. The screenshots provided in the thesis showcase the user-friendly interface of the Settings window, offering a visual representation of the configuration process. These settings are foundational to the system's functionality, providing users with the flexibility to adapt the application to specific hardware configurations and experimental setups. The inclusion of these screenshots serves to enhance the clarity and comprehensibility of the thesis content, elucidating the meticulous attention given to system customization and parameterization.
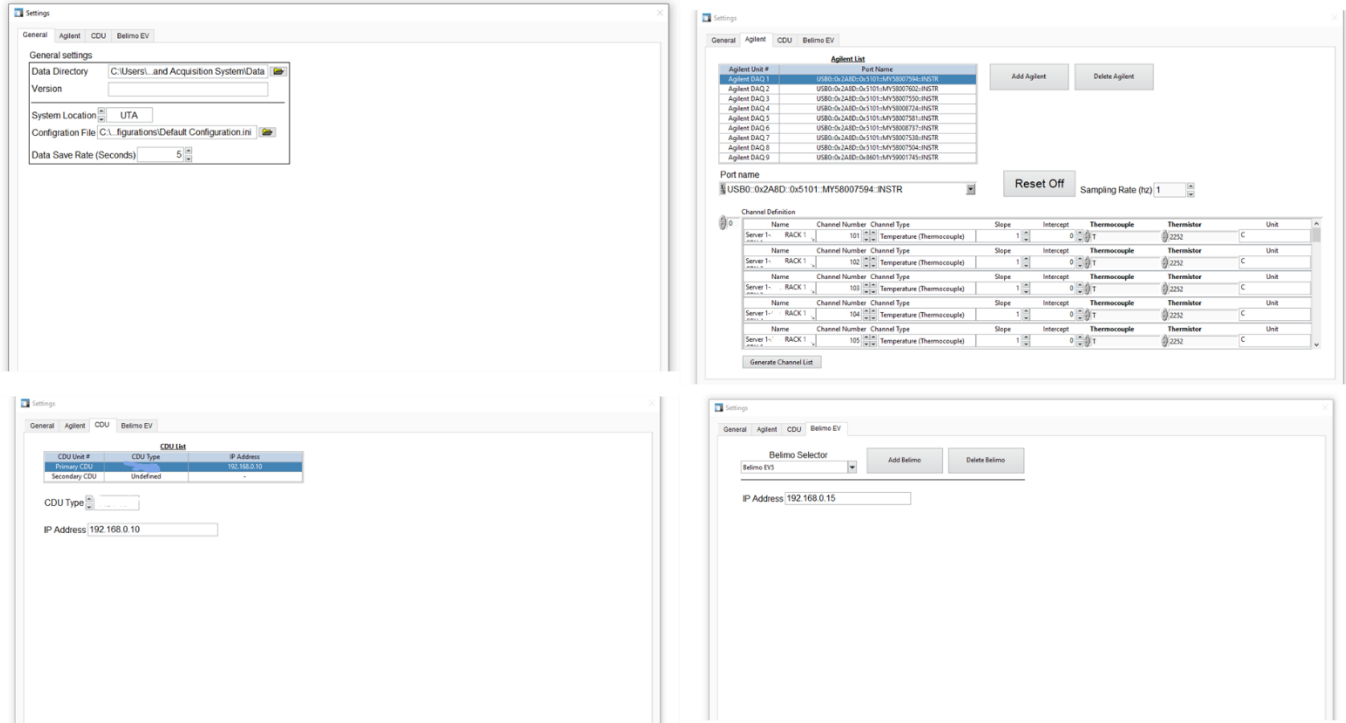
FIGURE 5.3: Settings window

The System Configuration window within the application plays a pivotal role in tailoring the software to meet the specific requirements of the experimental setup. This window becomes instrumental after defining key parameters such as DAQ ports, DAQ channel mapping, Belimo and CDU IP addresses, ensuring a seamless transition to the configuration phase. Within this window, users can meticulously set up the structure of the Data Center, specifying essential details such as the number of racks, DAQs in use, type of CDU, count of Belimo valves, and power supplies. Each rack is individually defined with the allocated number of servers, associated Belimo valve, and sensors assigned to designated DAQ channels. Moreover, users have the flexibility to establish a nomenclature for all the racks, enhancing clarity and organization. The provided screenshot of the System Configuration window visually encapsulates the versatility and user-friendly nature of this critical stage, showcasing the software's adaptability to diverse experimental setups and its capacity to streamline the configuration process for optimal system performance.
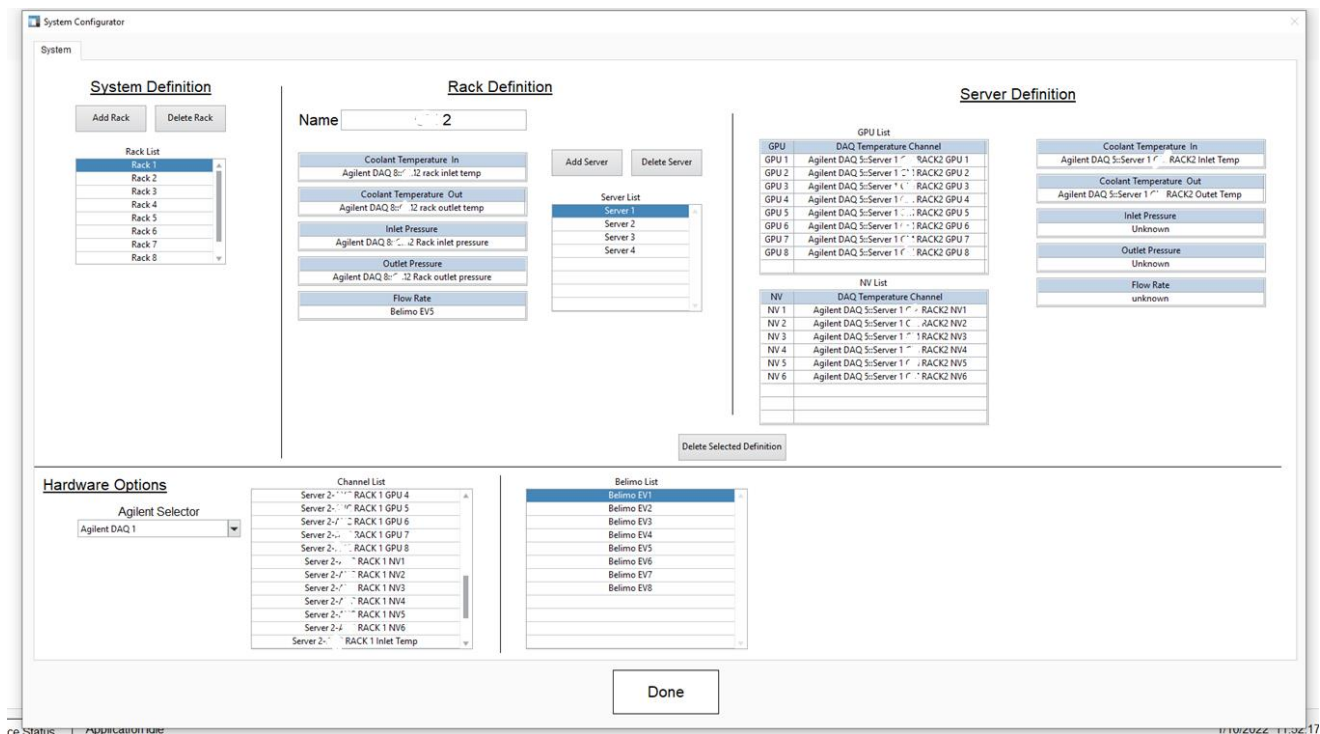
FIGURE 5.4: System configuration window

The specified path serves as the repository for all configuration files, encapsulating the essence of the system's flexibility and adaptability. Within this designated folder, users have the ability to create and store multiple configurations tailored to diverse experimental setups. Notably, the file named "default configuration" assumes significance as it automatically loads upon initiating the application. This streamlined approach simplifies the user experience, ensuring that the software seamlessly launches with a predetermined baseline configuration. The emphasis on a centralized folder for configuration files underscores the software's commitment to facilitating efficient management and retrieval of user-defined setups, promoting a user-friendly and accessible approach to system customization and initialization.
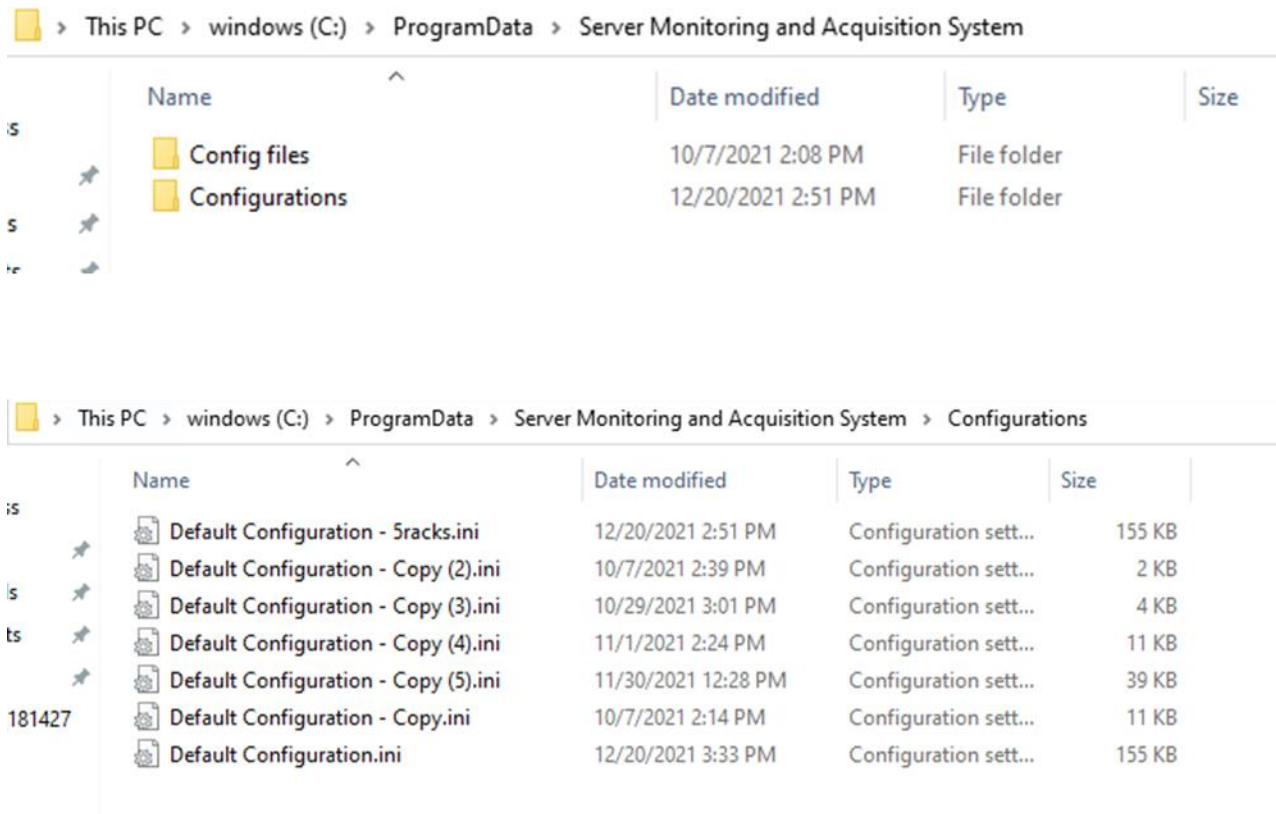
FIGURE 5.5: Configuration file path

The "View System" panel serves as a comprehensive layout overview for the Data Center within the application. It provides a crucial tool for monitoring the operational status of servers, racks, and the Cooling Distribution Unit (CDU) against predefined limits. Users can easily assess whether these components are functioning within specified parameters. The configuration within the "View System" panel includes the definition of limits for racks and servers, allowing for precise control and monitoring.

Furthermore, the application incorporates the GAR (Graphical Analysis of Risks) model to facilitate time-critical risk assessment. This model aids in generating clear communication regarding potential risks associated with the experimental setup. The integration of the GAR model ensures a proactive approach to risk management, allowing users to identify and address potential issues promptly.

Figure 5.6 provides a visual representation of the "View System" panel, showcasing the real-time status of servers, racks, and the CDU. Figure 5.6 illustrates the GAR model limits established for servers and racks, reinforcing the application's commitment to providing users with a holistic view of the system's health and risk factors. This dual-image presentation effectively communicates the practical application of the "View System" panel in conjunction with the GAR model for comprehensive risk assessment within the context of liquid cooling system experimentation.
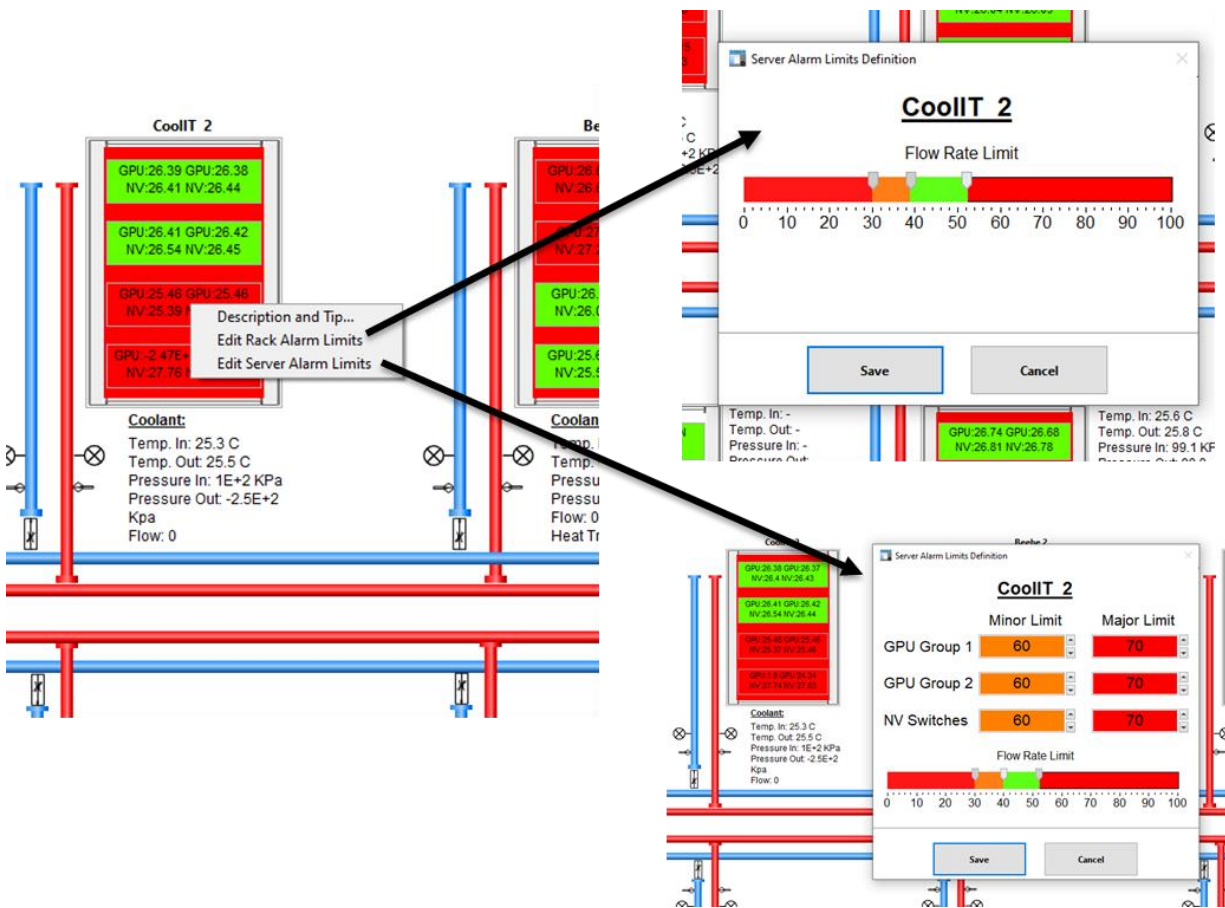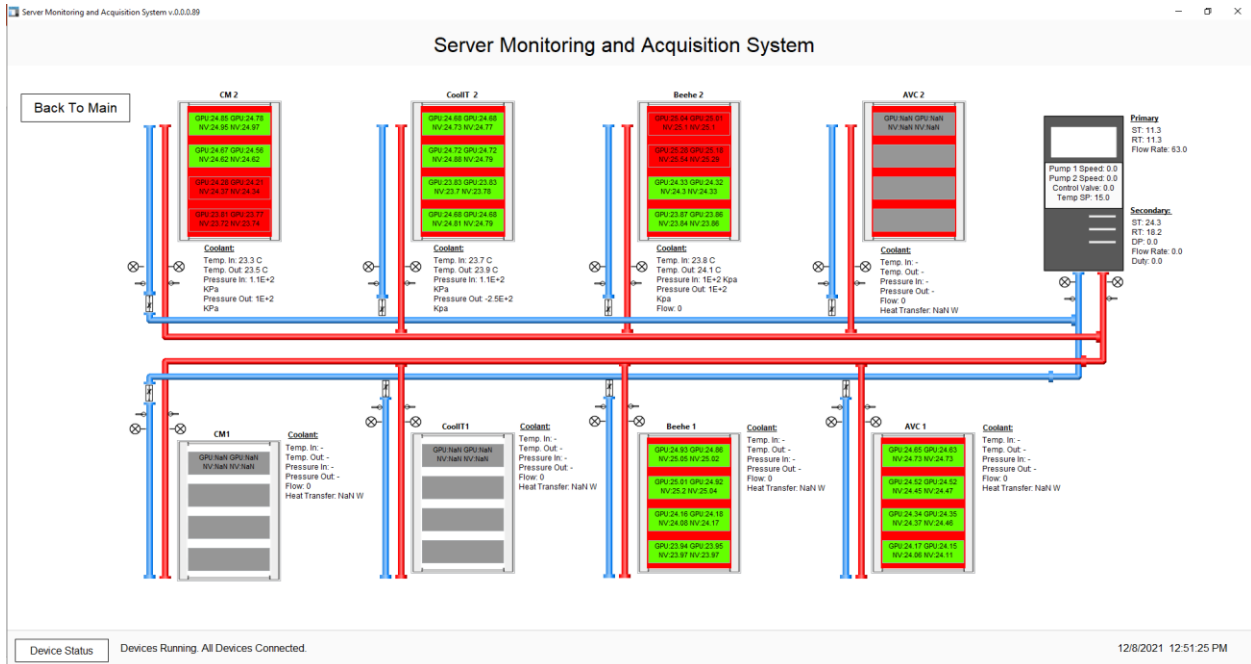
FIGURE 5.6: SYSTEM PANEL DEPICTING GAR MODEL

Clicking on any specific rack within the application navigates the user to the dedicated "Rack Analysis" window, as depicted in the provided image. This tab serves as a detailed analytical space where users can access real-time plots, including Delta P vs. time, Flow rate vs. time, and Heat transfer vs. time. These dynamic plots offer a comprehensive visual representation of critical performance metrics over time, aiding in the in-depth analysis of the rack's behavior.

In addition to the real-time plots, the "Rack Analysis" window provides essential information about the selected rack. This includes key parameters such as flow rate to the rack, inlet and outlet temperatures of the rack, as well as the inlet and outlet pressures of the rack. Furthermore, a server list is presented, furnishing users with a detailed breakdown of the servers associated with the selected rack.

The integration of this analytical window enriches the user experience by offering a focused and detailed examination of individual racks, facilitating informed decision-making and troubleshooting. The combination of real-time plots and critical information in this tab empowers users to gain valuable insights into the performance and conditions of specific racks within the liquid cooling system.
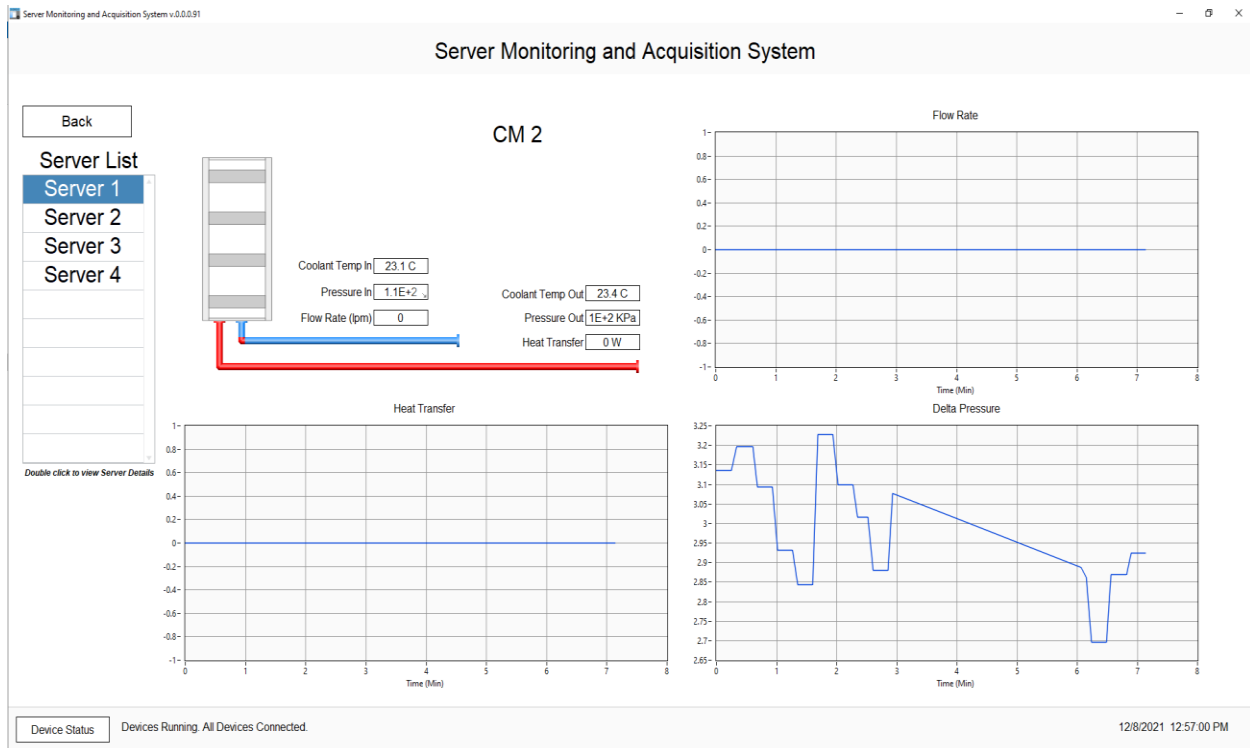
FIGURE 5.7: RACK TAB

Double-clicking on a specific server within the selected rack leads to the dedicated "Server Analysis" window in the LabVIEW application, as illustrated in the provided image. This tab provides a focused and detailed analysis of the individual server's performance. Within this window, users have access to real-time plots depicting critical parameters such as Delta P vs. time, Flow rate vs. time for the server, and GPU temperature vs. time.

The dynamic plots enable users to monitor and analyze the server's behavior in real-time, offering insights into the variations and trends of key performance metrics. The Delta P vs. time plot provides information on pressure differentials, the Flow rate vs. time plot illustrates fluid flow characteristics, and the GPU temperature vs. time plot offers a view of the server's thermal dynamics.

This server-centric analysis window enhances the granularity of the monitoring and diagnostic capabilities, empowering users to gain a deeper understanding of the specific server's response within the liquid cooling system. The real-time visualization of critical parameters facilitates effective troubleshooting, performance optimization, and informed decision-making in the context of server-level analysis.
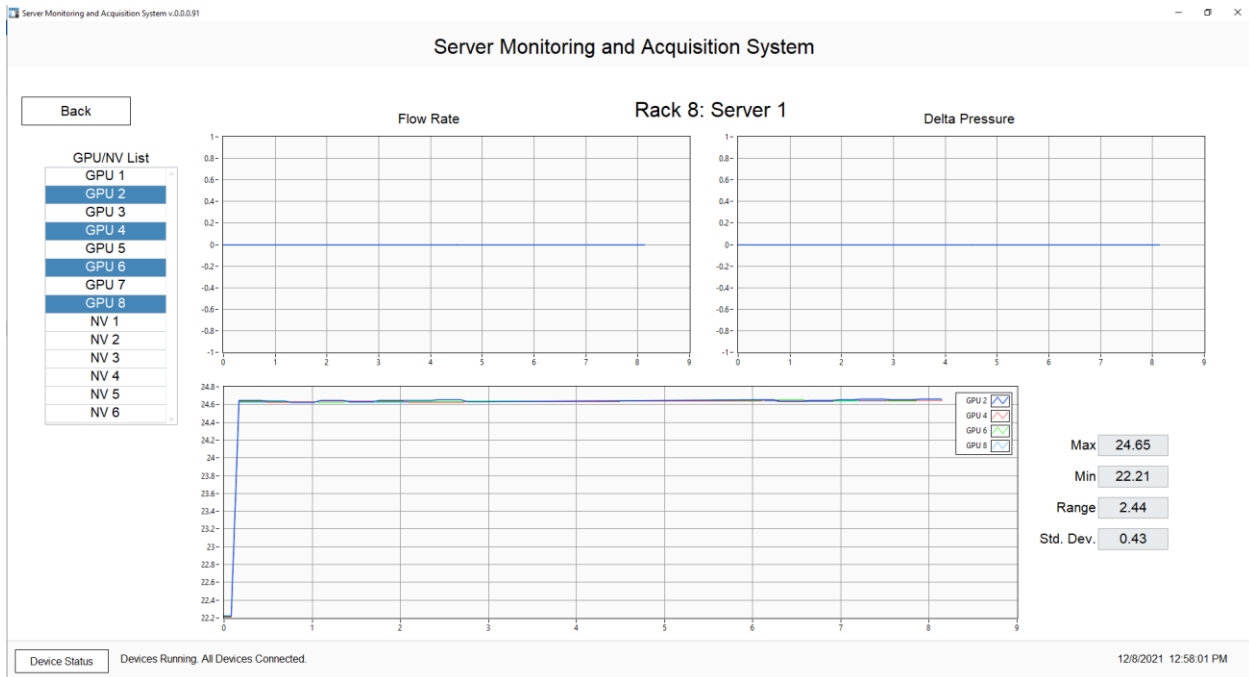

FIGURE 5.8: SERVER TAB

The "Belimo Valve" window within the LabVIEW application serves as a centralized hub for monitoring the status and parameters of connected Belimo valves. This window provides an overview of the number of Belimo valves currently connected to the system. Upon selecting a specific Belimo valve, the interface dynamically displays detailed information, including flow rate, inlet and outlet temperatures, valve position, and other relevant parameters associated with the selected Belimo valve.

Figure 5.9 illustrates this functionality, showcasing the user interface of the "Belimo Valve" window. This intuitive design enables users to efficiently navigate and access crucial information about individual Belimo valves. The detailed parameters presented in this window contribute to a comprehensive understanding of the performance and conditions of each Belimo valve within the liquid cooling system. The inclusion of such a dedicated window enhances the user experience by facilitating targeted monitoring, diagnostics, and control of Belimo valves, essential components in the efficient operation of the liquid cooling infrastructure.
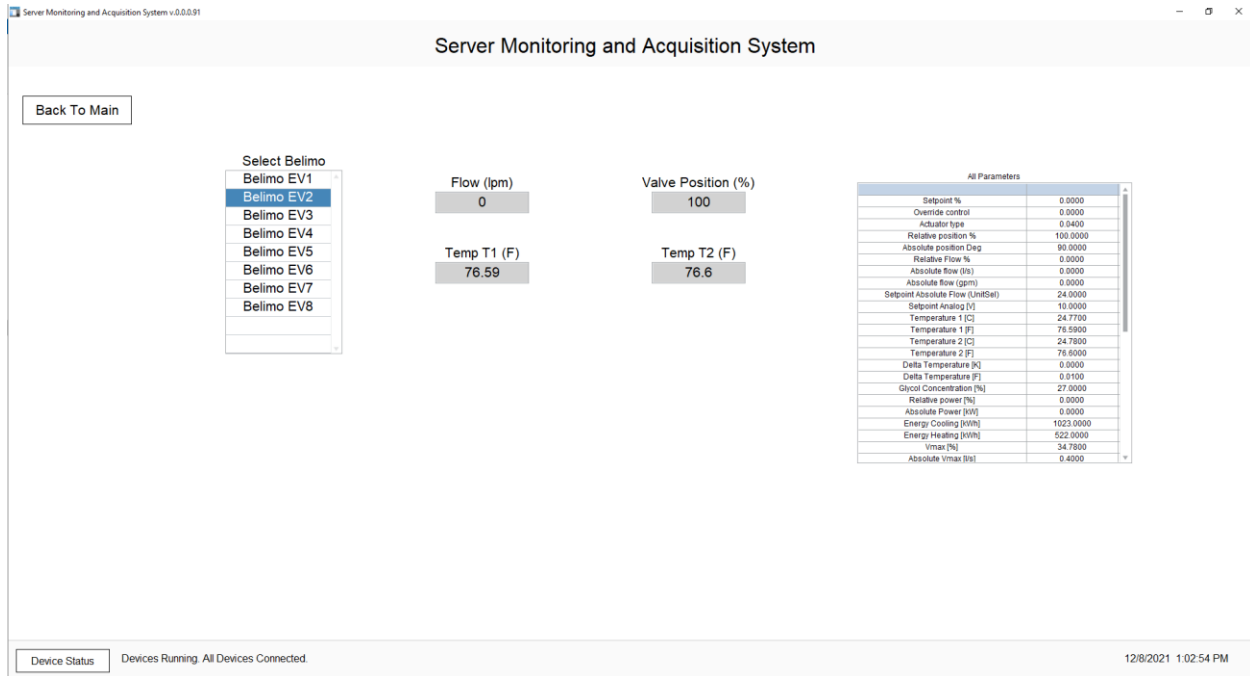
FIGURE 5.9: BELIMO VALVE TAB

The "View Plots" analysis window is a comprehensive visualization tool within the LabVIEW application, as depicted in the provided image. In this window, users have the capability to observe and analyze data from every sensor, Cooling Distribution Unit (CDU), Belimo valves, and power supplies. The interface is designed to present a holistic view of the system's performance, providing real-time data for a thorough analysis.

One of the notable features of this window is the ability to compare different plots simultaneously. Users can overlay and compare data from various sensors, CDUs, Belimo valves, and power supplies, allowing for a detailed examination of correlations and variations across different components of the liquid cooling system.

The intuitive design of the "View Plots" analysis window enhances the user's ability to make informed decisions, troubleshoot issues, and gain insights into the overall performance of the system. By consolidating data from multiple sources and enabling comparative analysis, this window plays a crucial role in facilitating a comprehensive understanding of the dynamic behavior of the liquid cooling infrastructure.
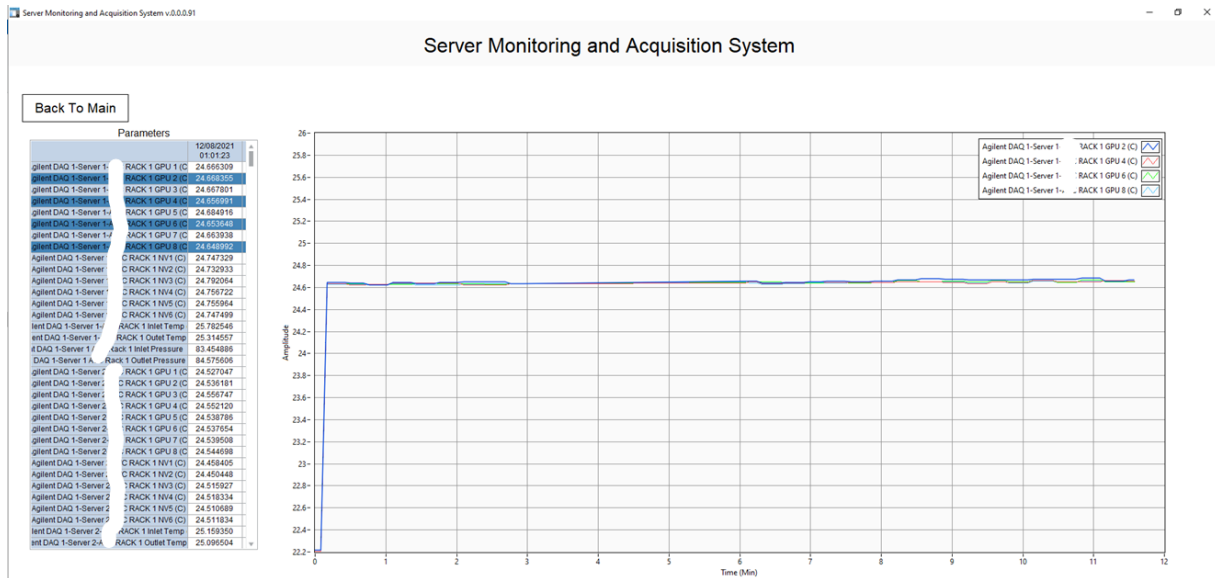
39

FIGURE 5.10: VIEW PLOT WINDOW

5.5 Future work

The future work for this project involves two key aspects aimed at further enhancing the capabilities of the liquid cooling system monitoring application. First, there is a plan to automate the system's hardware to enable seamless initiation and termination of the liquid-cooled data center operations. This automation would contribute to improved efficiency, reduced manual intervention, and increased overall system reliability. The implementation of automated start and stop procedures would align with the broader industry trend of integrating smart and autonomous functionalities into data center management.

Additionally, there is a focus on expanding the application's compatibility and functionality by integrating new equipment and sensors. This involves incorporating support for a diverse range of hardware components and extending the application's sensor capabilities to enhance data collection. By staying adaptable to emerging technologies and accommodating a broader array of equipment, the application aims to remain at the forefront of liquid cooling system monitoring.

These future developments signify a commitment to evolving the application to meet the evolving needs of liquid-cooled data centers, addressing both automation requirements and the integration of cutting-edge hardware solutions and sensors.

References

[1]   A. Shehabi et al., "United States Data Center Energy Usage Report," 2016.

[2]   Y. Hadad, S. Rangararajan, K. Nemati, B. Ramakrishnann, R. Pejman, P. R. Chiarot, B. Sammakia,, "Performance analysis and shape optimization of a water-cooled impingement micro-channel heat sink including manifolds," International Journal of Thermal Sciences, vol. 148, no. ISSN 1290-0729, p. 106145, 2020.

[3]   R. Schmidt, "Packaging of new servers-energy efficiency aspects," in Proc. 1st Berkeley Symp. Energy Efficient Electron., Berkeley, CA, USA, Jun. 2009, pp. 1–35. [Online]. Available: https://e3s-center.berkeley.edu/wp-content/uploads/2017/07/RogerSchmidt.pdf

[4]   Incropera, F., Liquid Cooling of Electronic Devices by Single-Phase Convection, John Wiley & Sons (New York, 1999), pp. 125-163.

[5]   S. V. Garimella & V. Singhal (2004) Single-Phase Flow and Heat Transport and Pumping Considerations in Microchannel Heat Sinks, Heat Transfer Engineering, 25:1, 15-25, DOI: 10.1080/01457630490248241

[6]   V. Torreblanca, A. Soto and D. Kulkarni, 2019, "Design and Testing of Liquid Cooled Thermal Solution for High Loading Processors," 18th IEEE Intersociety Conference on Thermal and Thermomechanical Phenomena in Electronic Systems (ITherm), Las Vegas, NV, USA, 2019, pp. 965-975. doi: 10.1109/ITHERM.2019.8757362

[7]   Kisitu, Deogratius, and Alfonso Ortega. "Thermal-Hydraulic Analytical Models of Split-Flow Microchannel Liquid-Cooled Cold Plates With Flow Impingement." In International Electronic Packaging Technical Conference and Exhibition, vol. 85505, p. V001T02A015. American Society of Mechanical Engineers, 2021.

[8]   Ramakrishnan, B., Hadad, Y., Alkharabsheh, S., Chiarot, P. R., and Sammakia, B. (July 12, 2019). "Thermal Analysis of Cold Plate for Direct Liquid Cooling of High Performance Servers." ASME. J. Electron. Packag. December 2019; 141(4): 041005. https://doi.org/10.1115/1.4044130.

[9]   Gharaibeh, Ahmad R., Yaman M. Manaserh, Mohammad I. Tradat, Firas W. AlShatnawi, Scott N. Schiffres, and Bahgat G. Sammakia. "Using a Multi-Inlet/Outlet Manifold to Improve Heat Transfer and Flow Distribution of a Pin Fin Heat Sink." Journal of Electronic Packaging 144, no. 3 (2022): 031017.

[10]   Gharaibeh, Ahmad R., Mohammad I. Tradat, Srikanth Rangarajan, Bahgat G. Sammakia, and Husam A. Alissa. "Multi-objective optimization of 3D printed liquid cooled heat sink with guide vanes for targeting hotspots in high heat flux electronics." International Journal of Heat and Mass Transfer 184 (2022): 122287.

[11]   Y. Hadad, S. Rangararajan, K. Nemati, B. Ramakrishnann, R. Pejman, P. R. Chiarot, B. Sammakia,, "Performance analysis and shape optimization of a water-cooled impingement micro-channel heat sink including manifolds," International Journal of Thermal Sciences, vol. 148, no. ISSN 1290-0729, p. 106145, 2020.

[12]   Y. Hadad, N. Fallahtafti, L. Choobineh , C. H. Hoang, V. Radmard, P. R. Chiarot, B. Sammakia, "Performance Analysis and Shape Optimization of an Impingement Microchannel Cold Plate," IEEE TRANSACTIONS ON COMPONENTS, PACKAGING AND MANUFACTURING TECHNOLOGY, vol. 10, no. 8, pp. 1304-1319, 2020.

[13]   Shahi, Pardeep, Apurv Deshmukh, Hardik Yashwant Hurnekar, Satyam Saini, Pratik Bansode, and Dereje Agonafer. "Numerical Investigation on Effect of Target Coolant Delivery in Liquid-Cooled Microchannel Heat Sinks." Journal of Enhanced Heat Transfer 30, no. 1 (2023). 016.

[14]   Shalom Simon, Vibin, Himanshu Modi, Krishna Bhavana Sivaraju, Pratik Bansode, Satyam Saini, Pardeep Shahi, Saket Karajgikar, Veerendra Mulay, and Dereje Agonafer. "Feasibility Study of Rear Door Heat Exchanger for a High Capacity Data Center." In International Electronic Packaging Technical Conference and Exhibition, vol. 86557, p. V001T01A018. American Society of Mechanical Engineers, 2022.

[15]   K. Hazelwood et al., "Applied machine learning at Facebook: A datacenter infrastructure perspective," in Proc. IEEE Int. Symp. High Perform. Comput. Archit. (HPCA), Feb. 2018, pp. 620–629.

[16]   V. K. Arghode, V. Sundaralingam, and Y. Joshi, "Airflow management in a contained cold aisle using active fan tiles for energy efficient data-center operation airflow management in a contained cold aisle using active fan tiles for energy efficient data-center," Heat Transf. Eng., vol. 37, nos. 3–4, pp. 246–256, Oct. 2016, doi: 10.1080/01457632.2015.1051386.

[17]   Allahverdyan, Armen E., Karen V. Hovhannisyan, Dominik Janzing, and Guenter Mahler. "Thermodynamic limits of dynamic cooling." Physical Review E 84, no. 4 (2011): 041109.

[18]   Boucher, Timothy D., David M. Auslander, Cullen E. Bash, Clifford C. Federspiel, and Chandrakant D. Patel. "Viability of dynamic cooling control in a data center environment." Journal of electronic packaging 128, no. 2 (2006): 137-144.

[19]   P. Shahi, S. Saini, P. Bansode and D. Agonafer, "A Comparative Study of Energy Savings in a Liquid-Cooled Server by Dynamic Control of Coolant Flow Rate at Server Level," in IEEE Transactions on Components, Packaging and Manufacturing Technology, vol. 11, no. 4, pp. 616-624, April 2021, doi: 10.1109/TCPMT.2021.3067045.

[20]   Heydari, Ali, Pardeep Shahi, Vahideh Radmard, Bahareh Eslami, Uschas Chowdhury, Chandraprakash Hinge, Lochan Sai Reddy Chinthaparthy et al. "A Control Strategy for Minimizing Temperature Fluctuations in High Power Liquid to Liquid CDUs Operated at Very Low Heat Loads." In International Electronic Packaging Technical Conference and Exhibition, vol. 86557, p. V001T01A011. American Society of Mechanical Engineers, 2022.

[21]   S. C. Mohapatra and D. Loikits, "Advances in liquid coolant technologies for electronics cooling," Semiconductor Thermal Measurement and Management IEEE Twenty First Annual IEEE Symposium, 2005., San Jose, CA, USA, 2005, pp. 354-360, doi: 10.1109/STHERM.2005.1412204.

[22]   C. -U. Kim et al., "Corrosion in Liquid Cooling Systems with Water-Based Coolant – Part 2: Corrosion Reliability Testing and Failure Model," 2020 19th IEEE Intersociety Conference on Thermal and Thermomechanical Phenomena in Electronic Systems (ITherm), Orlando, FL, USA, 2020, pp. 429-434, doi: 10.1109/ITherm45881.2020.9190565.

[23]   Aittomaki, A., A. Lahti, "Potassium Formate as a Secondary Refrigerant", Int J. Refrig., Vol. 20, No 4, pp. 276-282, 1997.

[24]   2001 ASHRAE HANDBOOK FUNDAMENTALS, American Society of Heating, Refrigerating and Air-Conditioning Engineers, Inc. (Atlanta, 2001), pp. 21.1-21.13.

[25]   D. A. Jones, Principles and Prevention of Corrosion, Prentice-Hall, Upper Saddle River, NJ, 1966.

[26]   P. R. Roberge, Corrosion Engineering – Principles and Practice, McGraw Hill, 2008

[27]   Guidelines for using propylene glycol- based heat transfer fluids in ... Accessed May 9, 2023. https://www.opencompute.org/documents/guidelines-for-using-propylene-glycol-based-heat-transfer-fluids-in-single-phase-cold-plate-based-liquid-cooled-racks-final-pdf.

[27]   Guidelines for using propylene glycol- based heat transfer fluids in ... Accessed May 9, 2023. https://www.opencompute.org/documents/guidelines-for-using-propylene-glycol-based-heat-transfer-fluids-in-single-phase-cold-plate-based-liquid-cooled-racks-final-pdf.

[28]   Mohapatra, Satish C. "An overview of liquid coolants for electronics cooling." Electronics cooling 12, no. 2 (2006): 22.

[29]   Pardeep Shahi, Ali Heydari, Chandraprakash Hinge,et al.., Analysis of Single-Phase Liquid Coolants for Direct-to-Chip Cold Plate Cooling in High-Performance Computing Systems." Proceedings of the ASME 2023 International Technical Conference and Exhibition on Packaging and Integration of Electronic and Photonic Microsystems. ASME 2023 International Technical Conference and Exhibition on Packaging and Integration of Electronic and Photonic Microsystems. San Diego, California, USA. October 24–26, 2023. V001T01A001. ASME. https://doi.org/10.1115/IPACK2023-110576

[30]   Shahi, P, Heydari, A, Eslami, B, Radmard, V, Hinge, C, Modi, H, Chinthaparthy, LSR, Tradat, M, Agonafer, D, & Rodriguez, J. "Methodology to Characterize Row Manifolds for High Power Direct to Chip Liquid Cooling Data Centers." Proceedings of the ASME 2023 International Technical Conference and Exhibition on Packaging and Integration of Electronic and Photonic Microsystems. ASME 2023 International Technical Conference and Exhibition on Packaging and Integration of Electronic and Photonic Microsystems. San Diego, California, USA. October 24–26, 2023. V001T01A002. ASME. https://doi.org/10.1115/IPACK2023-110587

[31]   Hu, G., J. Yang, and X. Zheng. "Corrosion behavior of aluminum cold plate in ethylene glycol coolant." Corros. Prot. 38, no. 11 (2017): 871-876.